FINAL TECHNICAL REPORT

U.S. Geological Survey External Grant
Award Numbers G21AP10270, G21AP10271, and G21AP10272

Grant Period: July 1, 2021 to May 31, 2023

MAPPING AND NEOTECTONIC INVESTIGATION OF THE SAWTOOTH FAULT, CENTRAL IDAHO: COLLABORATIVE RESEARCH WITH IDAHO GEOLOGICAL SURVEY, IDAHO STATE UNIVERSITY, AND BGC ENGINEERING, INC.

Submitted by

Zachery M. Lifton[1], Mark S. Zellman[2], and Glenn D. Thackray[3]

October 6, 2023

[1]Idaho Geological Survey, Idaho Water Center, Suite 201, 322 E. Front Street, Boise, ID 83702, http://www.idahogeology.org, zlifton@uidaho.edu, 208-364-4099

[2]BGC Engineering, Inc., Suite 300, 600 12th Street, Golden, CO, 80401, https://www.bgcengineering.ca/, mzellman@bgcengineering.ca, 720-617-3163

[3]Idaho State University, Department of Geosciences, 921 S. 8th Ave, Mail Stop 8072, Pocatello, ID 83209-8072, https://www.isu.edu/geosciences, thacglen@isu.edu, 208-282-3871

This material is based upon work supported by the U.S. Geological Survey, National Earthquake Hazards Reduction Program, through USGS NEHRP award numbers G21AP10270 (2021), G21AP10271 (2021), and G21AP10272 (2021). The views and conclusions contained in this document are those of the authors and should not be interpreted as representing the opinions or policies of the U.S. Geological Survey. Mention of trade names or commercial products does not constitute their endorsement by the U.S. Geological Survey.

TABLE OF CONTENTS

FIGURES

TABLES

APPENDICES

ABSTRACT

The Sawtooth fault is a Basin and Range normal fault in central Idaho, and a crustal source fault in the USGS National Seismic Hazard Model (NSHM). The presence of scarps in late Pleistocene glacial deposits and disturbance intervals found in moraine-bound lake sediment cores show that the fault has moved repeatedly during the late Quaternary. However, only a few studies have investigated the fault, and lidar coverage previously only existed for two small areas on its central section. Many of the best expressed fault scarps lie within protected wilderness and are difficult to access. These limitations have resulted in significant uncertainties for important parameters for seismic hazard modeling such as length, slip rate, and rupture length.

The March 31, 2020, moment magnitude (Mw) 6.5 Stanley earthquake occurred ~18 km north of the currently mapped northern terminus of the Sawtooth fault. The earthquake caused liquefaction and lateral spread at Stanley Lake, widespread shaking, local rockfall, landslides, and avalanches. The event likely occurred on an unknown fault and may have involved the Eocene trans-Challis fault system, which intersects the northern end of the Sawtooth fault. The moment tensor solution for the earthquake indicates it was a strike slip event, but aftershocks are aligned along the northern projection of the coarsely mapped northern Sawtooth fault and its presumed hanging wall. How the Sawtooth fault relates to the trans-Challis fault system and this earthquake is currently unknown.

We mapped the entire fault system in detail, provide much greater detail and identified additional fault length in comparison with the 60-km-long trace used in the NSHM, which is based on coarse-scale, pre-lidar, reconnaissance-level mapping. Previous detailed mapping was limited to only two small areas where lidar coverage intersects the fault, extended through aerial photographic analysis. Our detailed mapping of Quaternary fault scarps creates a basis on which to assess the fault geometry parameters. We have added to limited landform ages in order to better constrain slip rates.

This investigation has addressed major uncertainties related to earthquake history and earthquake potential of the Sawtooth fault: the fault length, geometry, scarp height, rupture length, and postglacial slip rates. We assessed fault length and rupture patterns with lidar data, coupled with terrestrial cosmogenic nuclide exposure dating of glacially deposited boulders along the range front.

Our new mapping reveals a more complex fault geometry, including parallel branches and previously unknown fault scarps such as those of the nearby west-dipping Cape Horn fault and southwest dipping Shake Creek fault. The southern half of the Sawtooth fault has a dearth of preserved scarps. The 13 cosmogenic exposure ages we collected from post-glacial surfaces displaced by the Sawtooth fault yielded ages from ~15 ka to ~19 ka. We calculated vertical slip rates of 0.21 +0.06/-0.08 mm/yr, 0.19 +0.06/-0.03 mm/yr, and 0.15 +0.03/-0.02 mm/yr (considered equivalent rates within rounding error and uncertainty) at sites in Iron Creek, Crooked Creek, and Smiley Creek basins, respectively.

INTRODUCTION

On March 31, 2020, a moment magnitude (Mw) 6.5 earthquake occurred approximately 9.5 km to 17 km ((Liberty et al., 2020; Pollitz et al., 2020; Wilbur, 2022; Montana Bureau of Mines and Geology, 2023; USGS, 2023a) north of the coarsely mapped northern extent of the Sawtooth fault (Figure 1). The earthquake resulted in liquefaction and lateral spreading at Stanley Lake, widespread shaking, local rockfall, landslides, and avalanches (Idaho Geological Survey, 2020). Moment tensor solutions for this earthquake suggest oblique left-lateral strike slip movement on a north-northwest striking fault or oblique right-lateral strike slip movement on an east-northeast striking fault. Although a strike slip event within the extensional Basin and Range Province is somewhat surprising, it is not unprecedented. A focal mechanism from the M6.6 1934 Hansel Valley earthquake in northern Utah also shows strike slip movement (Doser, 1989), a result of its transtensional setting (Bruno et al., 2017). The epicenter of the 2020 event plots close to the northeast trending Eocene trans-Challis fault system (TCFS) (Bennett, 1986), and aftershocks have occurred along a narrow trend projecting north beyond the northern end of the Sawtooth fault (Liberty et al., 2020; Pollitz et al., 2020; Yang et al., 2021; Luo et al. 2022; Wilbur, 2022). However, the relationship between the mapped Sawtooth fault and the unmapped structure(s) responsible for the M6.5 earthquake is not clear. This earthquake, and its associated effects and aftershocks, illustrate the current limited understanding of the Sawtooth fault in particular and the northern Basin and Range in general.

There are significant data gaps and a high degree of uncertainty for the key parameters used to characterize the Sawtooth fault in seismic hazard models. This is because very few prior studies have investigated the fault and available lidar data has been limited to two small areas near the central part of the fault. In addition, the recent March 31, 2020, M6.5 earthquake north of the Sawtooth fault highlights our limited understanding of how this fault relates to adjacent active structures.

This study addresses questions about the following important seismic hazard parameters of the Sawtooth fault which are either not constrained by prior information or highly uncertain. The parameters this study addresses are: (1) fault length, geometry, and scarp vertical separation (2) rupture length, and (3) postglacial slip rate. The results of this study provide new information about the Sawtooth fault that will improve the crustal fault seismic hazard parameters for the National Seismic Hazard Model (Hatem et al. 2022).

This investigation also begins to address broader scientific questions regarding complex rupture at the tips of normal faults, how those ruptures accommodate extension in the Basin and Range province and how the Sawtooth fault relates to the adjacent active structures. We have completed the first step in this analysis, specifically determining the map expressions of fault patterns near those fault tips and the spatial relationships to the TCFS on the northern end of the Sawtooth fault system and the Boulder Front fault at the southern end of the Sawtooth system. Earthquakes such as the 2020 M6.5 Stanley event, which did not occur on a mapped Quaternary fault or produce surface rupture, are important because they are strong enough to cause damage but may not be represented in the historical or paleoseismic records (Bruno et al., 2017). Understanding how these types of earthquakes relate to the mapped long-term geomorphic expression of the fault may provide better constraints on seismic hazards.

We focused on three objectives to help characterize the Sawtooth fault, leveraging existing data and new high-resolution lidar topographic data:

1. Conducted detailed mapping of the surface trace of the fault to evaluate the length and geometry of the surface trace as a basis for assessing fault length, rupture length, and siting of future investigation (e.g., paleoseismic trenching) sites.
2. Completed an along-strike analysis of fault scarps through digital elevation model (DEM) -based topographic profiles to characterize post-glacial fault activity, determine patterns of fault slip, and define sections of the fault with unique slip histories.
3. Collected and analyzed 13 terrestrial cosmogenic nuclide (TCN) exposure age samples to date key faulted glacial landforms that constrain the age of movement and slip rate on the Sawtooth fault.

The Sawtooth fault provides an excellent opportunity to evaluate the seismic hazard of a Basin and Range normal fault. Fault scarps and areas along strike of the projected surface trace are within the boundary of the Sawtooth National Recreation Area and almost entirely free from development and anthropogenic alteration. Multiple cycles of Quaternary glaciation have resulted in an accumulation of sediment and the development of geomorphic surfaces, deposits, and landforms of variable age along the range-front, most recently during the late Quaternary Pinedale glacial cycle (Gosse et al., 1995; Thackray et al., 2004; Sherrard, 2006). These deposits and features have been offset (repeatedly in some cases) by slip events on the Sawtooth fault. The boulders within the range-front glacial deposits originate from footwall granitic rocks, and thus are ideal for TCN exposure dating. Though they are not a focus of this proposal, range-front lakes enclosed by glacial moraines have trapped sediment deposited since deglaciation. These lakes are well-suited to record strong shaking events in disturbance intervals that can provide high-fidelity timing (e.g., Shapley et al., 2023; Johnson, 2010; Shapley and Finney, 2015). Although lake-derived data are indirect records, they can be compared against direct evidence of faulting in potential future paleoseismic trenches.

GEOLOGIC SETTING

The Sawtooth fault is located in central Idaho, ~7 km southwest of the town of Stanley, Idaho and ~114 km northeast of Boise, Idaho (Figure 1). As shown in the USGS *Quaternary Fault and Fold Database* (USGS, 2023b), the northwest trending normal fault is mapped for a length of 60 km along the eastern base of the Sawtooth Mountains where it vertically offsets late Quaternary glacial and alluvial deposits described in Thackray et al. (2004). At its northern end, geologic mapping by Fischer et al. (1992) and Kiilsgaard et al. (2006) show the Sawtooth fault terminating against the northeast trending TCFS, a 24-km-wide zone of normal faults that accommodated northwest-southeast Eocene extension associated with the Challis Volcanics eruptive episode (Bennett, 1986).

Regionally, the Sawtooth fault is within the northern Basin and Range Province where northeast-southwest extensional forces are accommodated generally by northwest trending normal faults. This area is referred to as the Centennial Tectonic Belt (Stickney and Bartholomew, 1987). The Centennial Tectonic Belt encompasses many of Idaho's Quaternary active faults within a broad southwest-northeast swath, north of the Snake River Plain. Of these, the nearest major Quaternary

active normal fault to the Sawtooth fault is the Lost River fault, which ruptured the surface in 1983 during an M 6.9 earthquake (Crone et al. ,1987). It is ~ 75 km to the east. The Boulder Front fault, which offsets late Pleistocene sediments, is closer, at a distance of ~10 km (Figure 1). It is southeast of, slightly oblique to the strike of, and oppositely dipping to the currently mapped southern end of the Sawtooth fault.

Some of the highest rates of seismicity in the state of Idaho occur within the Centennial Tectonic Belt (e.g., Dewey, 1987 and Stickney and Bartholomew, 1987). This includes several significant historic earthquakes with estimated epicenters located near the Sawtooth fault. On July 12, 1944, a M6.1 earthquake occurred 24 km northwest of Stanley, Idaho. Less than a year later, on February 13, 1945, a M6.0 earthquake occurred 45 km northwest of Stanley, Idaho. Those epicenters were relocated to that area, with large uncertainties, by Dewey (1987). On March 31, 2020, a third significant earthquake of similar size (M6.5) occurred less than 8 km and 17 km from the 1944 and 1945 events, respectively. All three of these earthquakes occurred north of the mapped extent of the Sawtooth fault. Although it is not clear if these earthquakes were associated with the Sawtooth fault, they are an indication of active tectonic processes in the area.

The Sawtooth fault was first recognized as a potential structural control on the Stanley Basin by Umpleby and Livingston (1920). It was later mapped by Reid (1963) and Kiilsgaard et al. 1970). There was some disagreement between early mappers of the Sawtooth fault regarding whether it offsets or is concealed by Quaternary glacial deposits. Tschanz et al. (1986) suggested that the Sawtooth fault offset surficial deposits, but their mapping, as well as mapping by Worl et al. (1991), Fischer et al. (1992) and Kiilsgaard et al. (2006), suggested that the fault is concealed by Quaternary glacial deposits. Geomatrix Consultants, Inc. (1989) evaluated the fault for a Bureau of Reclamation dam project on the Little Wood River that included a data review, aerial photograph interpretation, and aerial and ground reconnaissance. They identified and mapped at 1:250,000 scale Quaternary geologic and geomorphic features offset by the Sawtooth fault.

While previous mapping and studies of the Sawtooth Mountains and Stanley Basin have focused on bedrock and glacial geology (Tschanz et al., 1986; Thackray, 2008; Thackray et al., 2004), there have been few investigations focused on the neotectonics or paleoseismology of the Sawtooth fault. Detailed mapping of the fault scarp and tectonic geomorphology of the entire fault were incomplete. The fault trace used in the *NSHM* (Petersen et al. 2014; Hatem et al., 2022) is attributed to Reid (1963), who conducted reconnaissance mapping before modern satellite imagery and lidar topographic data were available. The USGS *Quaternary Fold and Fault Database* entry for the Sawtooth fault (Crone et al., 2010) does not specify the source of the fault trace mapping used in the current database. Thackray et al. (2013) mapped Sawtooth fault scarps for ~14 km from lidar, but that linework has not been incorporated into the IGS *Miocene and Younger Faults in Idaho* database (Breckenridge et al., 2003), USGS (2023) *Quaternary Fold and Fault Database*, or the *NSHM* (Hatem et al. 2022). Thus, a detailed map of Sawtooth fault Quaternary scarps remains unavailable.

Post-glacial scarps of the Sawtooth fault were documented by Thackray et al. (2013) using lidar data limited to small areas in the central and southern sections of the fault zone. The fault trace mapping was extended NW to Stanley Lake and SE to Alturas Lake using aerial photographs and field investigation. That study concluded that a) scarps in the central section of the fault zone near

Stanley are relatively continuous and 6.3 ± 1.5 m high in ~11-15 ka glacial landforms, suggesting 2-3 postglacial rupture events; b) scarps in the southern section of the fault zone (Pettit, Yellowbelly, and Alturas lakes) are less continuous; and c) few scarps are apparent in aerial photographs and satellite imagery NW of Stanley Lake. These relationships suggested three fault segments or sections of contrasting slip rate, but data remain insufficient to determine segmentation. Published gravity data (Mabey and Webring, 1983; Webring and Mabey, 1995) further suggest that the southern part of the fault bounds a deep, alluvium-filled basin. In contrast, the central and northern parts of the fault bound a shallower basin, suggesting long-term northwestward migration of fault activity (Thackray et al., 2013).

The timing of deglaciation of the range front is based on analysis of lacustrine sediment and limited TCN dating of moraine boulders in the Redfish Lake area. Sherard (2006) produced several TCN ages from moraine boulders in the Redfish Lake and Bench Lakes drainages. End moraines near the downvalley end of Redfish Lake date to 15-22 ka (ages recalculated using CRONUS version 3.0). Radiocarbon-dated lacustrine sediment reported in Mijal (2008) indicates that the cirques were deglaciated by ~14 cal ka and that the cirque glaciers terminated upvalley of the cirque lakes thereafter. Therefore, deglaciation is assumed to have occurred between 15 and 14 ka. However, the dated locations are several kilometers from the fault zone and are linked by inference to the deglaciation of the range front.

Shapley et al. (2023) used disturbed layers preserved in lacustrine sediment cores from Redfish Lake as evidence of two Holocene earthquakes (~4,300 cal yr BP and before 7,600 cal yr BP) in the middle portion of the Sawtooth fault. Lacustrine sediment cores from Pettit Lake, 15 km to the south, yielded evidence for a single postglacial earthquake at 5,100 cal yr BP that was distinct from the earthquake events at Redfish Lake.

In summer 2022 the USGS and collaborators from IGS and ISU excavated a paleoseismic trench across the Sawtooth fault at the Dutch Lake paleoseismic study site (Figure 1). This site is on the western branch of the northern section of the fault; at least one other fault branch parallels this to the east. They found evidence for a single-event rupture that displaces postglacial alluvial fan sediments ~2 m vertically. The complex fault zone exposed in the trench consists of several near-vertical strands that may accommodate normal-oblique motion (DuRoss et al., 2023

QUATERNARY GEOLOGY OF THE STUDY AREA

The study area lies at the foot of the Sawtooth Mountains, at the transition from the steep, range-front bedrock terrain to the structural basin of the Stanley Basin and Sawtooth Valley. The Sawtooth Range was heavily glaciated during successive Pleistocene glaciations, and the range front is largely buried in thick and extensive morainal deposits, with deglacial ground moraine and alluvial deposits occupying the valley floors of major drainages (Williams, 1961; Breckenridge et al., 1988; Sherrard, 2006; Thackray et al, 2004, 2013). Radiometric ages from ^{14}C (e.g., Thackray et al., 2004; Mijal, 2008) and CRN ages in Sherrard (2006, recalculated with revised production rates in Staley, 2015) indicate deglaciation of the range front between ~16 and 14 ka. However, the deglacial surfaces cut by Sawtooth fault scarps have not been directly dated, and that is a focus of this study.

The geomorphology of the Sawtooth Range and range front in the northern and southern parts of the fault zone contrasts with that of the central part. As noted, in the central part in particular, the range rises abruptly from the basin/valley floor. Range-front drainages there are deeply cut, terminal moraines generally lie several kilometers downvalley of the fault zone, and the fault primarily cuts deglacial valley floor ground moraine surfaces and high lateral moraines. In the northern section, the range is generally lower and drainages at the range front are shorter in length and less-well integrated, and only the major drainages are mantled by moraines and other direct glacial landforms. In the southern part of the fault zone, the drainages are deeply embayed, and the fault zone primarily includes terminal moraine complexes and proglacial outwash terraces.

New lidar data covering the entire fault zone permit detailed mapping of fault scarps and spatially associated glacial and fluvial landforms. In this report we describe fault scarp geometry along 65 km strike length, analyze spatial patterns of scarp height, map previously unrecognized fault scarps, and link the map data with new cosmogenic radionuclide ages on glacial landforms to constrain long-term fault slip rates.

INVESTIGATION METHODS

Lidar Compilation

An initial task of this project was to compile lidar data to support detailed desktop mapping and geomorphic analysis (Table 1). Two datasets provide freely available public lidar coverage for this project, and their merged extent is shown in Figure 1. This first lidar dataset is the 2005 Idaho State University (ISU) sponsored lidar collection that provides coverage two areas, one at Redfish Lake and another that covers the Yellow Belly Lake and Pettit Lake area. The second lidar dataset was sponsored by FEMA. It provides extensive coverage of the Sawtooth fault, and it was collected following the 2020 M6.5 Stanley earthquake. It covers the 2020 M6.5 Stanley earthquake epicentral area and the Sawtooth Mountain range front south to the Salmon River headwaters. The area around Yellow Belly and Pettit Lakes was not included in the FEMA lidar collection, but the data gap spatially overlaps with the 2005 ISU lidar collection.

The 2005 ISU lidar dataset can be downloaded in DEM format from the Idaho Lidar Consortium[1], and the FEMA lidar dataset can be downloaded in point cloud or DEM format from USGS LidarExplorer[2] or the Idaho Lidar Consortium.

[1] The Idaho Lidar Consortium can be accessed online at https://www.idaholidar.org/.
[2] The USGS LidarExplorer website can be accessed at

Table 1. Summary of Compiled Lidar

Lidar Project Name	Sponsor	Lidar Collection Date	Lidar Quality Level[1] (QL)
2018 Southern Idaho Lidar QL1	FEMA	2020, Post M6.5 Stanley, ID earthquake	QL1
2005 Sawtooths South	ISU	Oct 2005	QL3

Notes:

1. Lidar QL is defined by USGS (2022). QL1 data has a point spacing of ≤0.35 m and is suitable for a minimum DEM cell size of 0.5 m. QL3 data has a nominal point spacing of ≤1.41 m and is suitable for a minimum DEM cell size of 2 m.

Fault Scarp Mapping

We performed a desktop evaluation of lidar and mapped fault scarps in shapefile format at a scale of 1:10,000 using ESRI ArcGIS software. Active fault scarps were identified through desktop analysis of lidar based on geomorphic evidence described by Hansen et al. (1999) and McCalpin (2009). All mapped scarps were evaluated to exclude those formed by nontectonic processes such as erosion, gravitational slope failure, and those related to glaciation and older pre-Quaternary structures. In some locations, the Sawtooth fault scarps are intersected, adjacent to, or otherwise near features that fit the description of sackungen (McCalpin, 1999). These features can form due to nontectonic processes or as secondary features in response to an earthquake (McCalpin and Jones, 2021). Their surficial expression can be similar to that of a tectonic scarp, which makes them difficult to differentiate. Following the general geomorphic criteria defined by McCalpin (1999), we classified sackungen as scarps that dip opposite that of the main fault, are relatively short and arcuate, and restricted to a particular aspect of a slope. It is likely that some features are classified incorrectly, but this should have a minimal impact on the hazard characterization of the Sawtooth fault since their extent is limited. In general, the Quaternary fault scarps mapped in this study have a consistent geomorphic expression along strike, they are visible across one or more Quaternary deposits (i.e., alluvium, colluvium, glacial) or landform (i.e., alluvial fan, terrace, deglacial surface, moraine), and often increase in size on older surfaces.

All scarps were digitized systematically to ensure the linework represents the base of the scarp and so that the down-dip direction will be correctly indicated when symbolized in mapping software. Scarps were only digitized where they have geomorphic expression. We did not map scarps as inferred or buried where they are not visible in landforms such as active channels, terraces, waterbodies, or other locations. The attribute scheme is based on the Idaho State Geological Survey attribute scheme for fault scarps and is a work in progress (Table 2).

Table 2. GIS Attribute Schema for the Idaho Geological Survey's Active Fault Database

Field Name	Description	Data Type
OBJECTID	Automatic ESRI field	Object ID
Shape	Automatic ESRI field	Geometry
Id	Fault identification number	Long
FaultName	Fault name	Text
line_type	Mapped line type	Text
source	Source of mapping	Text
Shape_Leng	Length of line feature	Double
FaultAge	Age of fault	Text
SlipSense	Sense of slip	Text
DipDirecti	Fault dip direction	Text
SlipRate	Slip rate	Text
Mapper	Name of mapper	Text
MappingCon	Mapping confidence	Text
FaultNum	Fault number	Text
SectionNam	Fault section name	Text
FaultZone	Fault zone name	Text
StrandName	Fault strand name	Text
Synopsis	Synopsis	Text
Location_Comment	Location comments	Text
Geologic_Setting	Geologic setting	Text
Geomorph_Expression	Geomorphic expression	Text
Age_Youngest_Faulted_Dep	Age of youngest faulted deposit	Text
Detailed_Studies	Detailed studies	Text
IGS_Fault_Code	IGS fault code	Long
System_Code	Fault system code	Long
Structure_Code	Fault structure code	Long
System_Name	Fault system name	Text
Structure_Name	Structure name	Text
Compiler_and_Affil	Compiler and affiliation	Text
Shape_Length	Length of line feature	Double

Topographic Profiles

We selected 86 sites along the Sawtooth fault for extracting topographic profiles. Profile sites were chosen where the fault scarp is clearly expressed and where a simple landform is displaced. We avoided sites that were modified by erosion, or sites that included complicated surface landforms or complex surface faulting. At each point we drew profile lines approximately perpendicular across the scarp that captured surfaces on the hanging wall and foot wall of the fault. Profile lines

were positioned to follow the fall line down slope. We classified the offset surface at each profile site according to its apparent age into two broad age categories: pre-Last Glacial Maximum and post-Last Glacial Maximum. These classifications were determined by our interpretation of the character of the scarps, such as scarp height and steepness, and the stratigraphic relationships at each site.

The topographic profiles were extracted from bare earth lidar in ArcGIS Pro. We used the extracted data in a Matlab profiling tool developed by DuRoss et al. (2019). The profiling tool allows a user to define the upper, lower, and scarp face surfaces. Straight lines are fit to each surface and the vertical separation at the scarp is measured. The user can make multiple measurements with different interpretations and the profiling tool will calculate the median vertical separation value and uncertainties. We made five measurements of each profile.

We plotted the median vertical separation of each profile versus its along strike distance measured from south to north. Data were interpolated between points to give even point spacing. A moving average with a 2 km window was calculated to smooth the distribution of vertical separation along strike. Four outliers were excluded from the moving average (Sf-14, Sf-30, Sf-37, and Sf-47) because they are much larger than other values and crossed unusual deposits. Sf-14 crosses a large, uphill-facing scarp high up on an old moraine deposit, and Sf-30, Sf-37, and Sf-47 cross chaotic, hummocky deposits that we interpret to be older lateral moraines and/or landslides. We separated profile data on the main branch of the fault from data on the east branch and created moving averages for each. Both branches are plotted together on Figure 5.

Geochronology Sampling

Thirteen TCN boulder samples were collected for this study at three sites along the Sawtooth fault (Figures 2, 3, and 4).

Iron Creek Site

Iron Creek is a major drainage in the central section of the fault zone, lying between Redfish and Stanley lakes (Figure 2). Terminal Late Pleistocene moraines lie ~4 km downvalley of the fault zone and reflect two distributary ice lobes that split around a moraine or bedrock upland. The fault zone lies in an area of recessional terminal moraines and ground moraine, with minor outwash terraces flanking Iron Creek. In the fault zone, low-relief terminal and ground moraines are cut by a single fault scarp. A low (3-7 m) terminal moraine ridge lies ~1.5 km downvalley of the main fault scarp. The main fault scarp cuts a possible diffuse moraine ridge, but primarily lies in a sequence of ground moraine with poorly defined lateral moraine ridges. We collected seven TCN samples from erratic boulders in this drainage.

Crooked Creek Site

Crooked Creek lies adjacent to Iron Creek, with the valley floors separated laterally by ~2 km (Figure 3). Crooked Creek rises in a smaller drainage basin and its terminal moraines are only 3 km downvalley of the fault zone. Those latero-terminal moraines are truncated by moraines of the northern distributary ice lobe of Iron Creek. A single terminal recessional moraine lies

~0.6 km downvalley of the fault zone, and several lateral recessional moraines mark the southeastern margin of the valley. The fault cuts a low-relief ground moraine area with few defined moraine ridges. Isolated but common erratic boulders mark the ground moraine, however, and we collected four TCN samples from granitic boulders.

Smiley Creek Site

Smiley Creek is a NNE-trending drainage in the southern section of the Sawtooth fault zone (Figure 4). In comparison to the central section of the fault zone (e.g., Iron and Crooked creek study sites) Smiley Creek is a relatively low elevation, deeply embayed drainage. The fault zone there cuts the Late Pleistocene terminal moraine complex and associated proglacial outwash terraces downvalley of recessional moraines. We collected two TCN samples from erratic boulders in a low-relief terminal moraine complex within 200 m of the fault scarp.

TCN Sampling and Processing

All samples were taken from intact granitic boulders embedded in moraine or outwash surfaces. We selected boulders that appeared stable, with limited weathering and no evidence of being rolled over or exhumed since deposition. Each sample was approximately 20 cm long, 10 cm wide, and no more than 5 cm thick. Sample material was collected using an angle grinder, hammer, and chisel from the topmost surface of each boulder. The location, elevation, orientation, and surrounding horizon were recorded for each sample and used to calculate cosmogenic nuclide production rate and shielding factor (http://stoneage.ice-d.org/math/skyline/skyline_in.html).

Sample material was crushed and sieved to 250-500 µm at Idaho State University. The resulting material was sent to Lawrence Livermore National Lab's Center for Accelerator Mass Spectrometry (CAMS) for quartz isolation, beryllium extraction, and ^{10}Be measurement. The ^{10}Be concentrations and uncertainties from CAMS were used as input to version 3 of the CRONUS-Earth online exposure age calculator (http://hess.ess.washington.edu/math/) (Table 3). The exposure age calculator input also requires estimates for sample density and erosion rate. We used a sample density estimate of 2.65 g/cm^2 for all samples because it is a typical value for granite. Erosion rates are difficult to estimate, so we assumed 1 cm of erosion since the last deglaciation, which occurred approximately 15 ka. This yields an estimated erosion rate of 0.007 mm/yr.

Table 3. Sawtooth Fault CRONUS Exposure Calculator Input

```
SAWIC01 44.192450       -115.031620     2165    std     5       2.65    0.9902880.0007  2022;
SAWIC01 Be-10   quartz  316767  6058    07KNSTD;
SAWIC02 44.192517       -115.031550     2210    std     5       2.65    0.9902930.0007  2022;
SAWIC02 Be-10   quartz  301455  5864    07KNSTD;
SAWIC03 44.192467       -115.032117     2186    std     5       2.65    0.9902930.0007  2022;
SAWIC03 Be-10   quartz  309055  5905    07KNSTD;
SAWIC04 44.192817       -115.032333     2227    std     5       2.65    0.9902930.0007  2022;
SAWIC04 Be-10   quartz  314929  6596    07KNSTD;
SAWIC05 44.194633       -115.029817     2132    std     5       2.65    0.9942270.0007  2022;
SAWIC05 Be-10   quartz  304787  5029    07KNSTD;
SAWIC06 44.194550       -115.030050     2112    std     5       2.65    0.9942270.0007  2022;
SAWIC06 Be-10   quartz  321139  6138    07KNSTD;
SAWIC07 44.195150       -115.029233     2104    std     5       2.65    0.9942270.0007  2022;
SAWIC07 Be-10   quartz  310646  5109    07KNSTD;
SAWSC08 43.881500       -114.813000     2254    std     5       2.65    0.9741020.0007  2022;
SAWSC08 Be-10   quartz  368900  6021    07KNSTD;
```

```
SAWSC09 43.881467       -114.813067     2255    std     5       2.65    0.9919590.0007  2022;
SAWSC09 Be-10   quartz  372350  7253    07KNSTD;
SAWCC10 44.207417       -115.044583     2051    std     5       2.65    0.9830820.0007  2022;
SAWCC10 Be-10   quartz  304716  5738    07KNSTD;
SAWCC11 44.206400       -115.045000     2091    std     5       2.65    0.9830820.0007  2022;
SAWCC11 Be-10   quartz  285873  5541    07KNSTD;
SAWCC12 44.206333       -115.045033     2092    std     5       2.65    0.9830820.0007  2022;
SAWCC12 Be-10   quartz  285471  4919    07KNSTD;
SAWCC13 44.206450       -115.044750     2091    std     5       2.65    0.9828060.0007  2022;
SAWCC13 Be-10   quartz  297011  6049    07KNSTD;
```

Slip Rates

Based on our interpretation of the geomorphology and accessibility, we identified three sites for TCN sample collection and slip rate analysis: Iron Creek, Smiley Creek, and Crooked Creek (Figures 2-4). For each site, we combined vertical separation measurements from lidar-based scarp profiles and cosmogenic exposure ages from boulder samples to yield late Pleistocene vertical slip rate estimates. Slip rates were calculated using Zechar and Frankel's (2009) Matlab slip rate calculator, which allows multiple ages and displacement measurements to be used as input and propagates the uncertainties for both. For each site we calculated median vertical separation, median exposure age of displaced landform, and median slip rate.

RESULTS

Fault Mapping

The Sawtooth fault scarps mapped from lidar in this study are shown on Figures 6-9. Our detailed geomorphic map shows that scarps cut late Quaternary alluvial fan and glacial deposits for approximately 65 km along the eastern base of the Sawtooth Range. Previous maps of the fault (e.g., Fischer et al. 1992; Kiilsgaard et al.,2006; USGS, 2023) depict the Sawtooth fault as 60-km-long sinuous surface trace. Our new mapping shows the fault in greater detail, demonstrating fault complexities and providing evidence to define four sections of the fault. Herein, we use the term section to define portions of the fault based on geomorphic characteristics that may or may not be associated with segmented fault rupture. Those characteristics include abrupt fault strike changes, contrasts in the prevalence of scarps across landforms of contrasting ages, and presence of multiple parallel scarps. From south to north, the four segments are Salmon River to Alturas Lake (Figure 6), Alturas Lake to Decker Creek Section (Figure 7), Decker Creek to Stanley Lake (Figure 8), and a northern section that includes a western strand from Stanley Lake to at least Thatcher Creek and an eastern strand from Stanley Lake to Vader Creek (Figure 9).

In addition to mapping the Sawtooth fault, we identified, and mapped from lidar two additional previously unmapped, throughgoing scarps that exhibit strong geomorphic evidence for surface faulting. We refer to those features informally as the Cape Horn fault and the Shake Creek fault. In the following sections, we summarize our lidar-based fault mapping across the four sections of

the Sawtooth fault system, newly recognized scarps associated with the Cape Horn fault and Shake Creek fault, and other newly identified scarps of interest.

Salmon River to Alturas Lake Section

This is the shortest and southern-most section of the fault (Figure 6). Scarps are mapped for ~10-km, between the Salmon River on the east and Beaver Creek to the west. The scarps strike west-northwest, face to the north-northeast, and they form two main groups. The eastern group of scarps extends ~2.5 km from the Salmon River headwaters west to Frenchman Creek along a sinuous trend. The western scarp group is a linear to sinuous 3.5 km long section between Smiley Creek and the ridge that separates Little Beaver Creek from Beaver Creek. Between this point and Alturas Lake ~2.5 km to the northwest, a single ~400 m long northwest-trending scarp is mapped across the right moraine crest of the Alturas Lake valley. This scarp reflects a ~55° strike change from the southern scarps and, combined with the 2.5 km gap, defines the boundary between the Salmon River-Alturas Lake section and the Alturas Lake-Decker Creek section of the fault. To the southeast of the Salmon River-Alturas Lake section is the Boulder Front fault. The western-most exposed scarps of the west-southwest-dipping late Quaternary Boulder Front fault is ~6.5 km to the northeast and across Galena Summit from the scarps at Salmon River.

We performed field reconnaissance of the Salmon River to Alturas Lake Section and confirmed the presence of fault scarps at Frenchman Creek, Smiley Creek, and an unnamed tributary of Little Beaver Creek (Figure 7).

Alturas Lake to Decker Creek

This section of the fault is ~ 22-km-long and extends from an isolated 400-m-long, northwest trending scarp 2.5 km south of Alturas Lake to an isolated 800-m-long northeast-facing scarp at Decker Creek (Figure 8). The section is characterized by aligned, short (< 1 km), discontinuous scarps that face east-northeast except for one ~700-m-long scarp ~2.5 km southeast of Hell Roaring Lake that anomalously faces southwest. In the southern part of this section, mapped scarps are absent along a ~10.5-km-long area between Alturas Lake and Pettit Lake fault scarps. We consider three hypotheses to explain the absence of scarps in this portion of the fault 1) there is an actual absence of fault scarps in the geomorphic and surficial geologic record, 2) the expression of fault scarps across the vegetated and glaciation terrain in lidar data is below our threshold detection, and 3) fault scarps are present and have geomorphic expression, but they occur outside the extent of the lidar compiled for this study.

We conducted limited field reconnaissance of fault scarps in this section of the Sawtooth fault during this study.

Decker Creek to Stanley Lake

The Decker Creek to Stanley Lake section of the fault is characterized by a ~25-km-long, nearly continuous alignment of fault scarps along an arcuate trend that extends from an isolated ~800-m-long scarp at Decker Creek to ~4.5 km west of Stanley Lake in the north. Scarps strike north-northwest at the southern end, and west-northwest at the northern end (Figure 9). This section of the fault bounds the highest and most prominent portion of the of the Sawtooth Mountain

footwall block. Fault scarps in this section are constrained to a single alignment or narrow zone at steps or splays that cross late Quaternary alluvial fans, deglacial valley floors, morainal ridges, and high slopes that were not glaciated during the Pinedale glaciation.

We performed field reconnaissance for Quaternary fault scarps across the Iron Creek and Crooked Creek valley floors during this study, and Thackray et al., (2013) field checked scarps at several additional locations.

Stanley Lake to Thatcher Creek (west) and Vader Creek (east)

The northern-most section of the Sawtooth fault includes eastern and western branches (Figures 1 and 10). The boundary between the Decker Creek to Stanley Lake section and this section is marked by an abrupt ~50-60° clockwise strike change. At Elk Creek, the west-northwest zone of the Decker Creek to Stanley Lake scarps are juxtaposed against the north-northwest and north striking scarps within this section of the fault. Both strands intersect and overprint the northeast-trending Eocene TCFS. This differs from the mapping by Bennett (1986), Fischer et al. (1992), and Kiilsgaard et al. (2001) which show the Sawtooth fault as truncated against the TCFS. (Figure 1).

The scarps of the western strand trend north-northwest along a linear alignment from Elk Creek in the south to at least an unnamed tributary of Thatcher Creek in the north for a minimum length of ~12 km. The western strand could be as long as long as ~14 km, depending on if scarps along strike to the north and south are considered. The northern-most high confidence fault scarp in this group is a ~1.1-km-long, northwest trending, northeast facing scarp that intersects an unnamed tributary of Thatcher Creek. This scarp crosses deglacial Quaternary surfaces, landslides, and fluvial deposits and the Dutch Lake paleoseismic study site of DuRoss et al. (2023). A group of short, arcuate, and mostly uphill-facing scarps continue to the north, but we classified those features as sackungen. About 1.3 km north of the DuRoss et al. (2023) trench site we mapped a 1-km-long north-to-northeast trending scarp that we have classified as a queried fault scarp that could represent the northern-most mapped extent of the western strand if it is a fault scarp, rather than a scarp associated with gravitational or triggered slope failure.

The eastern strand is ~11.5-km-long and composed of discontinuous north-trending scarps from Elk Creek to Vader Creek. Uphill facing scarps on the east wall of the Elk Creek drainage could represent an additional 4 km of fault to the south if the scarps are related to surface faulting rather than gravitational or triggered slope failure. Between Elk Creek and Vader Creek, the eastern strand is characterized by a sinuous and stepping alignment of scarps across geomorphically complex late Quaternary surfaces and landforms that include striated deglacial valley floors, moraines, ice ablation, alluvial fans, and landslide terrain. At the northern end of the fault, the scarps bound the western margin of Flat Creek, cross the Vader Creek alluvial fan, and terminate near where Vader Creek intersects Idaho State Highway 21.

We performed field reconnaissance of Quaternary fault scarps on the eastern strand of the northern section at Flat Creek and at the Vader Creek alluvial fan (Figure 11).

Cape Horn fault

The Cape Horn fault is ~5 km west of the Sawtooth fault, and on the western side of the Sawtooth Mountain range (Figure 1). The fault is expressed as a ~10 km nearly continuous linear alignment of northwest-trending scarps that face west-southwest, opposite that of the Sawtooth fault. From south to north, the fault cuts late Quaternary alluvial-fan and glacial deposits of Canyon Creek, the broad Bench Creek and Banner Creek valley floors, then crosses a ridge through a broad notch, descends into and crosses the Cape Horn Creek valley, then climbs topography and becomes indistinct within landslide morphology (Figure 12).

Shake Creek fault

The Shake Creek fault is ~11 km from the northern end of the Sawtooth fault. Scarps associated with this fault strike north-northwest across a subalpine cirque at the head of Shake Creek (Figure 1 and 12) and vertically offset glacially striated surfaces. The fault is at least 1.8-km to possibly 3-km-long and expressed as a nearly continuous linear alignment of scarps that cross steep colluvium and striated late Pleistocene deglacial surfaces and deposits (Figure 13).

Other scarps of interest

Two other scarps or scarp groups of interest near the northern Sawtooth fault include:

- A ~1-km-long northeast trending scarp that is ~ 9 km north from the northern end of the Sawtooth fault and ~2.3 km southwest from the southern end of the Shake Creek fault scarp (Figure 1). The scarp dips east into the eastern slope of the Allen Creek drainage and forms a hillslope bench. At its southern end, it crosses notched ridge into the head of the Smith Creek drainage and becomes indistinct in a broad south-tending swale.
- A ~1.5-km-long alignment of scarps that cross the north-northwest trending ridge between Canyon Creek and divide between the North Fork of Canyon Creek drainage to the south and Bench Creek to the north (Figure 1). The scarps are ~3 km west of the western strand of the northern section of the Sawtooth fault and ~2 km southeast of the southern end of the Cape Horn fault. The scarps are oriented north-northeast and face south-southeast and they are within a swarm of short, arcuate, uphill facing scarps we classify as sackungen, but which are mapped as dikes by Fischer et al. (1992) and Kiilsgaard et al. (2001). They are oblique to faults Kiilsgaard et al. (2001) map along the southern margin of the TCFS. The 1.5-km-long alignment of scarps is unique because it 1) crosses the ridge, 2) follows the fall line on both sides of the ridge, and 3) continues as a linear trend across northeast trending bedrock structure until it becomes indistinguishable near the valley floor. Given the uncertainty of the origin of this feature, we have classified these scarps as queried fault scarps.

Topographic Profiles

In Figure 5, we plot individual vertical separation values measured from lidar at 86 topographic profile sites and their moving average for the 65-km-long Sawtooth fault. The moving average is helpful for smoothing out high frequency variation. We calculated and plotted separate moving averages for the main and east branches of the fault to account for cumulative fault slip on parallel strands. Individual vertical separation measurements range from ~1 m to nearly 10 m. The

distribution of vertical separation along the Sawtooth fault does not follow an idealized curve with a peak tapering off at either end, as seen in some other Basin and Range normal faults (e.g., DuRoss et al., 2019; Hampel et al., 2021). Instead, vertical separation along the Sawtooth fault appears to be uniformly distributed with a wide standard deviation. Patterns seen in the distribution on Figure 5 are mostly the result of the moving average calculation method and the distribution of the measurements along the scarp. The moving average lines in Figure 5 taper at the left side of each branch because the moving average starts at zero and has a window size of 2,000 m. We are testing additional methods of analysis, such as data padding and smaller window size, to account for edge effects. The dearth of vertical separation measurements between stations ~10,000 m and 38,000 m within the Alturas to Decker Creek section of the fault (Figure 5), and the resulting dip in the moving average, is caused by the relative absence of scarps between Alturas Lake and Decker Creek

While our coarse age categories likely mask some slip distribution patterns, we did observe age-offset relationships on lidar and in the field. In Crooked Creek, Iron Creek, and Fishhook Creek basins, we observed larger scarp heights across older landform surfaces. Deglaciated valley floors and fluvial terraces had scarps up to ~2 m high, while lateral moraines and older alluvial surfaces had scarps >4 m high. In some cases we observed very large (~10 m high) scarps high up on the range front on ridges and older moraines between glaciated valleys. Better age constraint on the many faulted surfaces along the Sawtooth range front would allow for a more detailed analysis of slip distribution. For example, dividing the scarp profiles into smaller age categories may yield clearer patterns in along strike slip. Or it may help test the hypothesis that progressively older surfaces have experienced greater cumulative slip.

Geochronology

We calculated ages and uncertainties for each sample and mean ages and uncertainties for our three sites. The CRONUS online exposure age calculator outputs three sets of results based on three production rate scaling models: “St”, a time-independent model based on Stone et al. (2000) and Lal (1991); “Lm”, a time-dependent model based on Lal (1991) and Nishiizumi et al. (1989); and “LSDn”, a time-dependent model based on Lifton et al. (2014). We use the LSDn model for our preferred results, and all the ages and slip rates we discuss herein are based on the LSDn model. We report results from all the production rate scaling models in Appendix A.

Table 4 summarizes the individual cosmogenic nuclide exposure ages and uncertainties by CRONUS. Samples ranged in age from ~14.8 ka to ~18 ka, which is consistent with the most recent deglaciation of the Sawtooth Range. The ages of our three study sites are described below and summarized in Table 5. The seven surface samples at the Iron Creek site have a median exposure age of 15.8 ± 1.3 mm/yr (1σ uncertainty). The four surface samples from the Crooked Creek site have a median exposure age of 15.9 +1.3/-1.2 mm/yr (1σ uncertainty). This age is indistinguishable from the calculated age at Iron Creek, and thus appear to reflect simultaneous deglaciation of the range front. This is consistent with broader deglacial ages calculated for the Redfish Lake drainage using data in Sherrard (2006) and Mijal (2008). The two surface samples from the Smiley Creek site have a median exposure age of 18.0 ± 1.2 mm/yr (1σ uncertainty). As expected from the geomorphic setting and relationships with the moraine sequence, these ages are

~2.5 ka older than the Iron Creek and Crooked Creek ages collected from deglacial/recessional landforms.

Table 4. Cosmogenic Nuclide Exposure Age Samples

Sample	Longitude (°E)	Latitude (°N)	Elev. (m)	Sample Thickness (cm)	Type	Be Concentration (atoms/g qtz)	Be 1σ Uncert. (atoms/g qtz)	Age* (a)	Age Uncert.* (a)
SAWIC01	-115.031620	44.192450	2165	5	Boulder, ^{10}Be	316767	6058	16063	1100
SAWIC02	-115.031550	44.192517	2210	5	Boulder, ^{10}Be	301455	5864	14770	1005
SAWIC03	-115.032117	44.192467	2186	5	Boulder, ^{10}Be	309055	5905	15401	1050
SAWIC04	-115.032333	44.192817	2227	5	Boulder, ^{10}Be	314929	6596	15228	1047
SAWIC05	-115.029817	44.194633	2132	5	Boulder, ^{10}Be	304787	5029	15751	1063
SAWIC06	-115.030050	44.194550	2112	5	Boulder, ^{10}Be	321139	6138	16903	1163
SAWIC07	-115.029233	44.195150	2104	5	Boulder, ^{10}Be	310646	5109	16420	1113
SAWSC08	-114.813000	43.881500	2254	5	Boulder, ^{10}Be	368900	6021	18042	1234
SAWSC09	-114.813067	43.881467	2255	5	Boulder, ^{10}Be	372350	7253	17864	1239
SAWCC10	-115.044583	44.207417	2051	5	Boulder, ^{10}Be	304716	5738	16966	1166
SAWCC11	-115.045000	44.206400	2091	5	Boulder, ^{10}Be	285873	5541	15382	1050
SAWCC12	-115.045033	44.206333	2092	5	Boulder, ^{10}Be	285471	4919	15348	1037
SAWCC13	-115.044750	44.206450	2091	5	Boulder, ^{10}Be	297011	6049	16015	1103

*Based on LSDn production rate scaling model.

Slip Rates

The slip rate results are summarized in Table 5 and Figure 14. When rounded to the nearest tenth of a millimeter per year (mm/yr), all three sites had a median vertical slip rate of 0.2 ± 0.1 mm/yr (1σ uncertainty). It is unclear if the vertical separations measured at these three sites represent one, two, or more rupture events. If this is one event, then these slip rates are calculated over an open interval and the rates do not accurately represent the long-term average. Paleoseismic trenching and further analysis of vertical separation may help resolve this question.

These rates are slow, but typical for many normal faults in the Basin and Range Province. The USGS Quaternary Fault and Fold Database (USGS, 2023b) previously estimated the Sawtooth fault slip rate to be <0.2 mm/yr based on offset Pinedale glacial deposits (Thackray et al., 2009). Thackray et al. (2013) estimated a vertical slip rate of approximately 0.5 mm/yr.

Table 5. Sawtooth Fault Slip Rate Data Summary

	Inputs				
Site	**Vertical Separation Profile ID**	**Exposure Age Sample ID**	**Median Vertical Separation and 1σ Uncertainty (m)***	**Median Age and 1σ Uncertainty (ka)***	**Median Slip Rate and 1σ Uncertainty (mm/yr)***
Iron Creek	Sf-45 Sf-46	SAWIC01 SAWIC02 SAWIC03 SAWIC04 SAWIC05 SAWIC06 SAWIC07	3.41 +0.87/-1.19	15.77 +1.31/-1.25	0.21 +0.06/-0.08
Crooked Creek	Sf-49 Sf-50 Sf-51	SAWCC10 SAWCC11 SAWCC12 SAWCC13	3.02 +0.95/-0.46	15.88 +1.34/-1.21	0.19 +0.06/-0.03
Smiley Creek	Sf-06 Sf-07 Sf-08	SAWSC08 SAWSC09	2.67 +0.45/-0.27	17.96 +1.24/-1.24	0.15 +0.03/-0.02

*We report results with two decimal places here because some values are very low. However, this is not the true precision as these are not significant figures. One decimal place (i.e., tenths of mm/yr) is a more realistic and appropriate level of precision for these results and we round results to that level when discussing them in the text. For slip rate uncertainty results less than 0.1 mm/yr that do not round up, we default to a value of 0.1 since uncertainty cannot be zero and 0.1 mm/yr is the lowest meaningful value.

SUMMARY AND CONCLUSIONS

This study addressed questions of fault geometry, paleo-earthquake timing, and fault slip rate. We conducted detailed fault scarp mapping, fault scarp topographic analysis, and exposure dating of faulted landforms. We expect the resulting maps, vertical separation measurements, ages, and slip rates will be important inputs for seismic hazard analyses such as the National Seismic Hazard Model.

Surface Length of the Quaternary Sawtooth Fault

The surface length of the Quaternary Sawtooth fault is defined by the presence of fault scarps on Quaternary landforms such as moraines, deglacial valley floors, terraces, and alluvial fans, and associated Quaternary alluvial, colluvial and fluvial deposits. We measured Quaternary faults scarps along the Sawtooth fault for a total length of at least 65 km along a sinuous fault zone. The scarps are mostly concentrated along a narrow fault zone or single scarp. Based on geomorphic characteristics of the scarp such as bends, steps, strike change, or gaps in scarps we define five fault sections. We do not yet have enough definitive paleoseismic information to relate these sections to fault rupture length and whether or not they represent fault segment boundaries.

The longest and most continuous alignment of scarps extends for 22 km from Decker Creek to Stanley Lake. The most complex section is the northern-most section from Stanley Lake to the north and includes two strands. DuRoss et al. (2023) trenched the western strand on an unnamed tributary of Thatcher Creek and found evidence for a single post Pinedale earthquake, and both strands intersect the northeast trending TCFS as mapped by Bennett (1986) and overprint the structure with late Quaternary north-northwest to north trending normal faulting.

Late Quaternary Paleoseismology of Sawtooth Fault

Existing paleoseismic data are limited on the Sawtooth fault. Geomorphic indicators, such as the steep range front, down-dropped basin, and youthful scarps cutting glacial deposits, are evidence of ongoing activity through the late Quaternary. Our interpretation of the fault geometry and geomorphology suggests the Sawtooth fault can be split into four sections. However, it is still unclear if these sections are true fault segments that behave differently. The only known paleoseismic trench was reported by DuRoss et al. (2023). They excavated a trench across the Sawtooth fault near Dutch Lake, exposing a complex, nearly vertical fault zone with evidence for one surface rupturing earthquake since the Last Glacial Maximum. Radiometric ages from the Dutch Lake trench are pending a manuscript in preparation. A handful of radiocarbon and cosmogenic exposure ages from past studies (Thackray et al., 2004; Mijal, 2008; Sherrard, 2006) constrain a limited number of glacial deposits along the Sawtooth Mountains range front. Those ages support a basic framework for understanding the timing of surface rupture. In addition, recent lacustrine paleoseismology work by Johnson (2010) and Shapley et al. (2023) has identified evidence for two Holocene earthquakes on the middle portion of the Sawtooth fault and a separate earthquake on the southern portion of the fault.

The results from this investigation add to the understanding of the paleoseismic history of the Sawtooth fault. Our preliminary analysis of scarp heights, combined with 13 cosmogenic exposure ages, yield vertical slip rates at three sites. Rounded to the nearest tenth of a mm/yr, all the slip

rates are 0.2 ± 0.1 mm/yr. These are slow slip rates, but well within the range of rates seen on other Basin and Range normal faults.

Future paleoseismic work can help resolve remaining questions about the Sawtooth fault. For example, further analysis of scarp heights may provide insight into the number of surface rupturing events along the fault. Additional geochronology data can also help determine if older landforms record progressively larger fault displacement. Paleoseismic trenching other sections and branches of the Sawtooth fault may help resolve its rupture history, including which parts of the fault have ruptured and when those events occurred. Paleoseismic trenches on nearby faults (e.g., the Boulder Front, Cape Horn, and Shake Creek faults) can also provide important information about whether they rupture with the Sawtooth fault. We identified five sites for potential future paleoseismic trenches (Figure 6, 10, and 12 and Table 6). These sites were chosen based on the size and quality of the scarp, feasibility for excavating a paleoseismic trench, and likelihood of securing landowner permission to conduct the study.

Table 6. Potential Future Paleoseismic Trench Sites

Site Name	Longitude	Latitude
Vader Creek Trench	-115.124006	44.345663
Bench Creek Trench	-115.230422	44.30885
Smiley Creek Trench	-114.809027	43.88061
Little Beaver Creek Trench	-114.817251	43.892595
Frenchman Creek Trench	-114.769634	43.869393

Relationship of the Sawtooth Fault or Other Nearby Scarps to the 2020 Mw 6.5 Stanley, Idaho Earthquake

The relationship of the 2020 Mw 6.5 Stanley, Idaho earthquake to the Sawtooth fault remains enigmatic. Studies by Liberty et al. (2020); Pollitz et al. (2020); Yang et al. (2021); Luo et al. (2022), and Wilbur et al. (2022) evaluated aftershocks and proposed various models of the source fault. Earthquake epicenters for the main shock reported by the USGS National Earthquake Information Center (USGS, 2023a), Wilbur et al. (2022), and the Montana Bureau of Mines and Geology (2023) all plot north of the Sawtooth fault. Focal mechanisms of the 2020 Stanley earthquake indicate oblique left-lateral movement on a north-northwest trending down-to-the-west fault, whereas the Sawtooth fault is a down-to-the-east normal fault. Thus, the location, geometry, and sense of motion of the 2020 Stanley earthquake are difficult to reconcile with a rupture on the Sawtooth fault.

During this study, we identified and mapped previously unrecognized Quaternary fault scarps that were not known to researchers and reconnaissance teams at the time of the earthquake. These newly recognized scarps include those associated with the northern Sawtooth fault, the Cape Horn fault, the Shake Creek fault, and other anomalous scarps of unknown origin within the 2020 Mw 6.5 epicentral region (Figures 1, 6, 10, 12, and 13). Some of these newly recognized scarps roughly coincide with modeled faults from aftershock data. For example, Fault 2 from Yang et al. (2021) and Fault 1 from Pollitz et al. (2020) dip west and are broadly similar to the Cape Horn fault. The

northeast trending Faults 2 and 3 from Pollitz et al. (2020) and Fault 3 from Yang et al. (2021) are broadly similar to the northeast trending questionable fault scarp we mapped southeast of the southern end of the Cape Horn fault. However, our field reconnaissance of the Cape Horn fault near Bench Creek and Banner Summit found no evidence of historical surface faulting. Likewise, our field reconnaissance of the eastern strand of the Sawtooth fault at Flat Creek and Vader Creek and observations by DuRoss et al. (2023) at the Dutch Lake site on the northern-most main strand of the fault found no evidence of historical surface rupture. Scarps along the Shake Creek fault, as well as other scarps mapped from lidar in this study and classified as questionable fault scarps have not been confirmed or evaluated through field-based reconnaissance. However, it is possible that the Mw 6.5 earthquake was small enough that it did not produce surface rupture (Wells and Coppersmith, 1994; Youngs et al., 2003). Finite fault models of the source fault by the USGS (2023a) come within ~1 km of the surface, but do not rupture the surface. The Idaho Geological Survey (2020) found no evidence of surface rupture when they performed field reconnaissance in the epicentral area.

PROJECT DATA

Data collected and generated in this investigation will be publicly available through several sources. Mapping will be published in the Idaho Geological Survey's active fault database, available as a webmap and GIS database on IGS's website: www.idahogeology.org. We are preparing this work for submission to a peer reviewed journal where the detailed mapping, topographic profile analysis, cosmogenic exposure age data, and slip rate data will be presented and made available through supplementary data files.

REFERENCES

Bennett, E.H., 1986, Relationship of the trans-Challis fault system in central Idaho to Eocene and Basin and Range extensions. Geology, 14(6), 481-484.

Breckenridge, R.M., Lewis, R.S., Adema, G.W., and Weisz, D.W., 2003, Miocene and younger faults in Idaho: Idaho Geological Survey Map 8, scale 1:1,000,000, 1 sheet.

Bruno, P.P.G., DuRoss, C.B., and Kokkalas, S., 2017, High-resolution seismic profiling reveals faulting associated with the 1934 Ms 6.6 Hansel Valley earthquake (Utah, USA): Geological Society of America Bulletin, v. 129, no. 9-10, p. 1227–1240, https://doi.org/10.1130/B31516.1.

Crone, A.J., Haller, K.M., and Lewis, R.S., compilers, 2010, Fault number 640, Sawtooth fault, in Quaternary fault and fold database of the United States: U.S. Geological Survey website, https://earthquakes.usgs.gov/hazards/qfaults, accessed 05/06/2020 10:42 AM.

Crone, A.J., Machette, M.N., Bonilla, M.G., Lienkaemper, J.J., Pierce, K.L., Scott, W.E., and Bucknam, R.C., 1987, Surface faulting accompanying the Borah Peak earthquake and segmentation of the Lost River fault, central Idaho: Bulletin of the Seismological Society of America, v. 77, p. 739–770.

Dewey, J.W., 1987, Instrumental seismicity of Central Idaho: Bulletin of the Seismological Society of America, v. 77, no. 3, p. 819-836.

Doser, D.I., 1989, Extensional tectonics in northern Utah– southern Idaho, U.S.A., and the 1934 Hansel Valley sequence: Physics of the Earth and Planetary Interiors, v. 54, p. 120–134, doi:10.1016/0031-9201(89)90192-1.

DuRoss, C. B., Bunds, M. P., Gold, R. D., Briggs, R. W., Reitman, N. G., Personius, S. F., and Toké, N. A., 2019, Variable normal-fault rupture behavior, northern Lost River fault zone, Idaho, USA. Geosphere, 15(6), 1869–1892. https://doi.org/10.1130/GES02096.1.

DuRoss, C.B., Lifton, Z.M., Hatem, A.E., Briggs, R.W., Jobe, J.A.T., Reitman, N., Thackray, G.D., Zellman, M.S., Collett, C.M. 2023. Geologic Context of the 2020 Mw 6.5 Stanley, Idaho Earthquake: Preliminary Paleoseismology of the Sawtooth Fault. Seismological Research Letters. V. 94, no. 2b, p. 1196.

Fischer, F.S., McIntyre, D.H., and Johnson, K.M. 1992. Geologic Map of the Challis 1° x 2° Quadrangle, Idaho. U.S. Geological Survey. Miscellaneous Investigation Series Map I-1819.

Geomatrix Consultants, Inc., 1989, Final report seismotectonic evaluation for Little Wood River Dam site: Technical report to U.S. Bureau of Reclamation, Denver, Colorado, 104 p., 2 pls.

Gosse, J.C., Klein, J., Evenson, E.B., Lawn, B., Middleton, R., 1995. Beryllium-10 dating of the duration and retreat of the last Pinedale glacial sequence. Science 268, 1329-1333.

Hansen, K.L., Kelson, K.I., Angell, M.A., and Lettis, W.R. (1999). Techniques for Identifying Faults and Determining Their Origins. Prepared for Division of Engineering Technology Office of Nuclear Regulatory Research. NUREG CR-5503.

Hatem, A. E., Collett, C. M., Briggs, R. W., Gold, R. D., Angster, S. J., Field, E. H., et al., 2022, Simplifying complex fault data for systems-level analysis: Earthquake geology inputs for U.S. NSHM 2023. Scientific Data, 9(1), 506. https://doi.org/10.1038/s41597-022-01609-7.

Idaho Geological Survey, 2020, Stanley Earthquake event page: Idaho Geological Survey website, accessed June 1, 2020, https://www.idahogeology.org/stanley-earthquake.

Hampel, A., Hetzel, R., and Erdmann, M.-S., 2021, Postglacial slip distribution along the Teton normal fault (Wyoming, USA), derived from tectonically offset geomorphological features: Geosphere, v. 17, no. 5, p. 1517– 1533, https://doi.org/10.1130/GES02370.1.

Johnson, E.M., 2010, Lacustrine evidence of seismic events on the Sawtooth Fault in the Redfish Lake Drainage, Sawtooth Mountains, Central Idaho [M.S. Thesis]: Idaho State University, 116 p.

Kiilsgaard, T.H., V.L. Freeman, J.S. Coffman. 1970. Mineral resources of the Sawtooth Primitive area, Idaho. U.S. Geological Survey Bulletin 1319-D, p. D1-D174.

Lal, D., 1991, Cosmic ray labeling of erosion surfaces: in situ nuclide production rates and erosion models. Earth and Planetary Science Letters, 104(2–4), 424–439. https://doi.org/10.1016/0012-821X(91)90220-C.

Liberty, L.M., Lifton, Z.M., and Mikesell, T.D., 2021, The 31 March 2020 Mw 6.5 Stanley, Idaho, Earthquake: Seismotectonics and Preliminary Aftershock Analysis.

Lifton, N., Sato, T., and Dunai, T. J., 2014, Scaling in situ cosmogenic nuclide production rates using analytical approximations to atmospheric cosmic-ray fluxes. Earth and Planetary Science Letters, 386, 149–160. https://doi.org/10.1016/j.epsl.2013.10.052.

Luo, B., Zhu, H., Yang, J., Lay, T., Ye, L., Lu, Z., and Lumley, D., 2022, Detecting and Locating Aftershocks for the 2020 Mw 6.5 Stanley, Idaho, Earthquake Using Convolutional Neural Networks. Seismological Research Letters, 93(6), 3266–3277. https://doi.org/10.1785/0220210341.

Mabey, D.R., and Webring, M.W., 1983, Regional geophysical studies in the Challis quadrangle, in McIntyre, E.H., ed., Symposium on the Geology and Mineral Deposits of the Challis 1°x2° quadrangle, Idaho: U.S. Geological Survey Bulletin 1658, p. 69–79.

McCalpin, J.P., 1999, Criteria for determining the Seismic Significance of Sackungen and Other Scarplike Landforms in Mountainous Regions *in* Hanson, K.L., Kelson, K.I., Angell, M.A., and Lettis, W.R., Techniques for Identifying Faults and Determining Their Origins. U.S., Nuclear Regulatory Commission. NUREG/CR-5503.

McCalpin, J.P., 2009, Paleoseismology (2nd ed.) San Diego, California. Academic Press.

McCalpin, J.P., and Jones, L.C.A., 2021, The Stillwater Scarp, Central Nevada, USA; Coseismic Gravitational Failure on a 1.200-M-High Range-Front Escarpment, Environmental Engineering Geoscience, Vo. XXVII, No. 4, pp. 377-393.

Mijal, B., 2008, Holocene and latest Pleistocene glaciation in the Sawtooth Mountains, central Idaho [M.S. thesis]: Western Washington University, 62 p.

Montana Bureau of Mines and Geology, 2023, Montana Regional Seismic Network earthquake catalog: International Federation of Digital Seismograph Networks. https://doi.org/10.7914/SN/MB.

Nishiizumi, K., Winterer, E. L., Kohl, C. P., Klein, J., Middleton, R., Lal, D., & Arnold, J. R., 1989, Cosmic ray production rates of ^{10}Be and ^{26}Al in quartz from glacially polished rocks. Journal of Geophysical Research, 94(B12), 17,907-17,915.

Petersen, M.D., Moschetti, M.P., Powers, P.M., Mueller, C.S., Haller, K.M., Frankel, A.D., Zeng, Yuehua, Rezaeian, Sanaz, Harmsen, S.C., Boyd, O.S., Field, Ned, Chen, Rui, Rukstales, K.S., Luco, Nico, Wheeler, R.L., Williams, R.A., and Olsen, A.H., 2014, Documentation for the 2014 update of the United States national seismic hazard maps: U.S. Geological Survey Open-File Report 2014–1091, 243 p., https://dx.doi.org/10.3133/ofr20141091.

Petersen, M.D., Shumway, A.M., Powers, P.M., Mueller, C.S., Moschetti, M.P., Frankel, A.D., Rezaeian, S., McNamara, D.E., Luco, N., Boyd, O.S. and Rukstales, K.S., 2019, The 2018 update of the US National Seismic Hazard Model: Overview of model and implications: Earthquake Spectra, 36(1), pp.5-41, https://doi.org/10.1177%2F8755293019878199.

Pollitz, F.F., Hammond, W.C., and Wicks, C.W., 2021, Rupture Process of the M 6.5 Stanley, Idaho, Earthquake Inferred from Seismic Waveform and Geodetic Data. Seismological Research Letters, 92(2A), 699–709. https://doi.org/10.1785/0220200315

Reid, R.R., 1963, Reconnaissance geology of the Sawtooth Range: Idaho Bureau of Mines and Geology Pamphlet 129, 37 p., 2 pls.

Shapley, M.D., and Finney, B.P., 2015, Lake morphometry controls the remobilization and long-term geochemical imprint of distal tephra deposition. Journal of Paleolimnology, v. 53, p. 309–320; DOI 10.1007/s10933-015-9826-6.

Shapley, M., Thackray, G.D., Johnson, E., and Finney, B., 2023, Lacustrine evidence reveals spatially and temporally distinct Holocene ruptures on the Sawtooth Fault, Central Idaho, USA. Journal of Quaternary Science, p. 1-16, https://doi.org/10.1002/jqs.3554.

Sherard, C., 2006, Regional correlations of Late Pleistocene climatic changes based on cosmogenic nuclide exposure dating of moraines in Idaho [M.S. thesis]: Western Washington University, 91 p.

Staley, A.E., 2015, Glacial geomorphology and chronology of the Quinault Valley, Washington, and broader evidence of Marine Isotope States 4 and 3 glaciation across northwestern United States: M.S. Thesis, Idaho State University, 177 p. https://geology.isu.edu/thesis.html

Stickney M.C. and Bartholomew M.J., 1987, Seismicity and late Quaternary faulting of the northern Basin and Range Province, Montana and Idaho: Bulletin of the Seismological Society of America, v. 77, p. 1602–1625.

Stone, J. O., 2000, Air pressure and cosmogenic isotope production. Journal of Geophysical Research: Solid Earth, 105(B10), 23753–23759. https://doi.org/10.1029/2000JB900181.

Thackray, G. D., 2008, Varied Climatic and Topographic Influences on Late Pleistocene mountain glaciation in the western United States. Journal of Quaternary Science, 23(6): 671-681.

Thackray, G.D., Lundeen, K.A., and Borgert, J.A., 2004, Latest Pleistocene alpine glacier advances in the Sawtooth Mountains, Idaho, USA: reflections of midlatitude moisture transport at the close of the last glaciation. Geology 32(3): 225-228. Doi: 10.1130/G20174.1

Thackray, G.D., Rodgers, D.W., Johnson, E.M., and Shapley, M.D. 2009. Preliminary evaluation of a newly discovered Holocene scarp on the Sawtooth Fault, central Idaho. Geological Society of America Abstracts with Programs, Vol. 41, No. 7, p. 55.

Thackray, G.D., Rodgers, D.W., and Streutker, D., 2013, Holocene scarp on the Sawtooth fault, central Idaho, USA, documented through lidar topographic analysis: Geology, v. 41, p. 639-642, doi:10.1130/G34095.1.

Tschanz, C.M., Kiilsgaard, T.H., and Seeland, D.A., 1986, Geology of the eastern part of the Sawtooth National Recreation Area, Idaho: U.S. Geological Survey Bulletin 1545-A, p. 17-43, 1 pl., scale 1:62,500.

Umpleby, J.B., and Livingston, D.C., 1920, A reconnaissance in south central Idaho embracing the Thunder Mountain, Big Creek, Stanley basin, Sheep Mountain, and Seafoam districts: Idaho Bureau of Mines and Geology Bulletin 3, 23 p.

U.S. Geological Survey (2022). Lidar Base Specifications 2022 rev. A. USGS. Accessed online on 11 Aug 2023 from https://www.usgs.gov/media/files/lidar-base-specification-2022-rev-a.

U.S. Geological Survey (2023a). M6.5 Stanley earthquake event page, available at https://earthquake.usgs.gov/earthquakes/eventpage/us70008jr5/executive (last accessed June 2023).

U.S. Geological Survey (USGS), 2023b, Quaternary fault and fold database for the United States, accessed June 2023, at: https://www.usgs.gov/natural-hazards/earthquake-hazards/faults.

Webring, M.W., and Mabey, D.R., 1995, Geophysical anomalies, in Fisher, F.S., and Johnson, K.M., eds., Geology and mineral resource assessment of the Challis 1°x2° Quadrangle, Idaho: U.S. Geological Survey Professional Paper 1525, p. 53–62.

Wells, D.L. and Coppersmith, K.J., 1994, New empirical relationships among magnitude, Rupture length, rupture width, rupture area, and surface displacement. Bulletin of the seismological Society of America, 84(4), 974-1002.

Wilbur, S.F., 2022, Machine-Learning Reveals Aftershock Locations for Three Idaho Earthquake Sequence: M.S. Thesis, Boise State University, Boise, Idaho, 110 p.

Williams, P.L., 1961, Glacial geology of the Stanley Basin: Moscow, Idaho Bureau of Mines and Geology, pamphlet 123, 29 p.

Worl, R.G., Kiilsgard, T.G., Bennett, E.H., Link, P.K., Lewis, R.S., Mitchell, V.E., Johnson, K.M., and Snyder, L.D., 1991, Geologic map of the Hailey 1° x 2° quadrangle, Idaho: U.S. Geological Survey Open-File Report 91-340, 1 sheet, scale 1:250,000.

Yang, J., Zhu, H., Lay, T., Niu, Y., Ye, L., Lu, Z., Luo, B., Kanamori, H, Huang, J., Li, Z., 2021, Multifault Opposing-Dip Strike-Slip and Normal-Fault Rupture During the 2020 M w 6.5 Stanley, Idaho Earthquake. Geophysical Research Letters, 48(10). https://doi.org/10.1029/2021GL092510.

Youngs, R.R., Arabasz, W.J., Anderson, R.E., Ramelli, A.R., Ake, J.P., Slemmons, D.B., McCalpin, J.P., Doser, D.I., Fridrich, C.J., Swan III, F.H. and Rogers, A.M., 2003, A methodology for probabilistic fault displacement hazard analysis (PFDHA). Earthquake Spectra, 19(1), pp.191-219.

Zechar, J.D. and Frankel, K.L., 2009, Incorporating and reporting uncertainties in fault slip rates. Journal of Geophysical Research, 114(B12), B12407. https://doi.org/10.1029/2009JB006325.

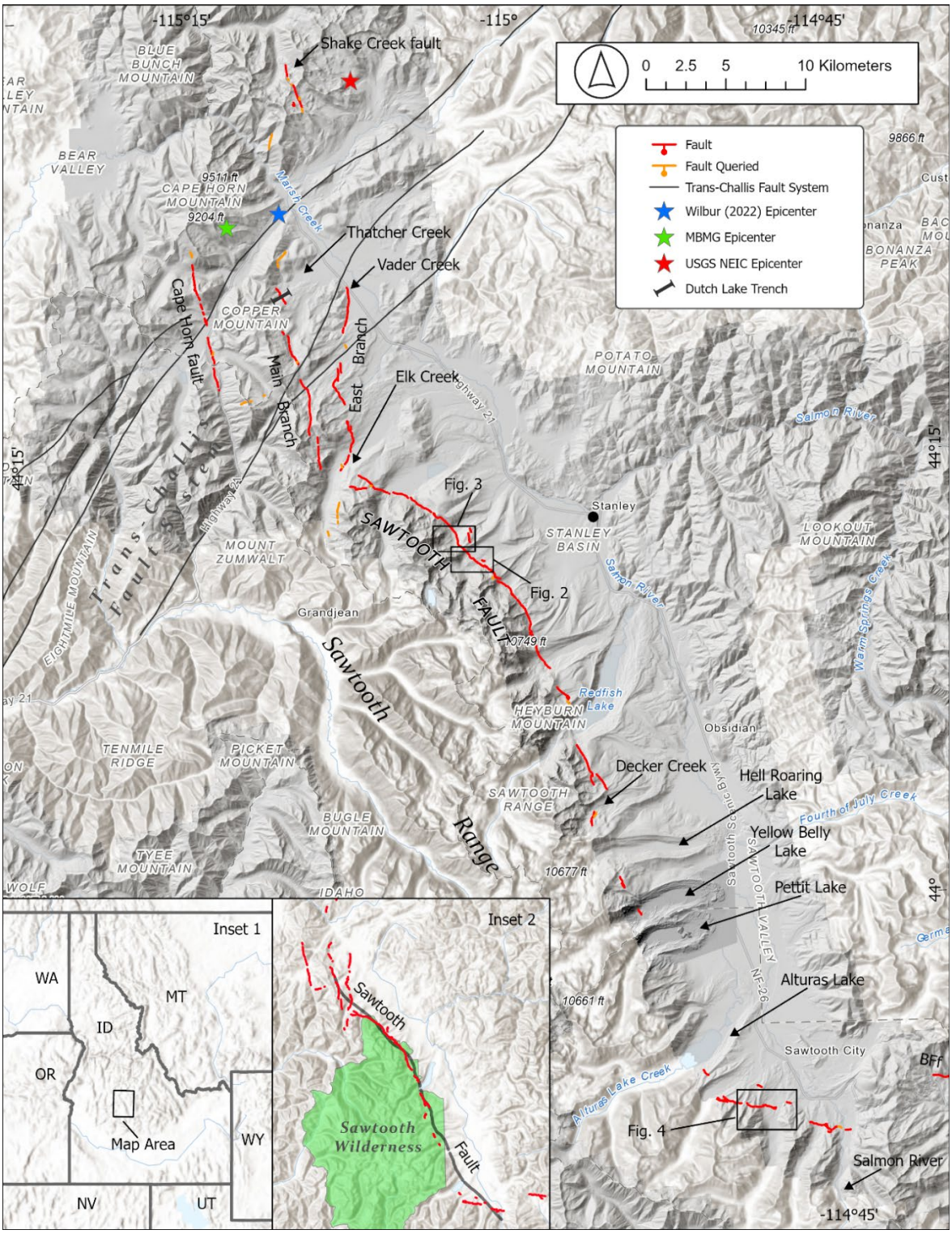

Figure 1. Overview map showing lidar basemap and new mapping of the Sawtooth fault. Colored stars are different locations of the 2020 M6.5 Stanley earthquake. Inset 2 shows the Sawtooth Wilderness boundary, and compares the previously mapped Sawtooth fault (gray line; USGS, 2023) with new mapping from this investigation (in red) BFf-Boulder Front fault.

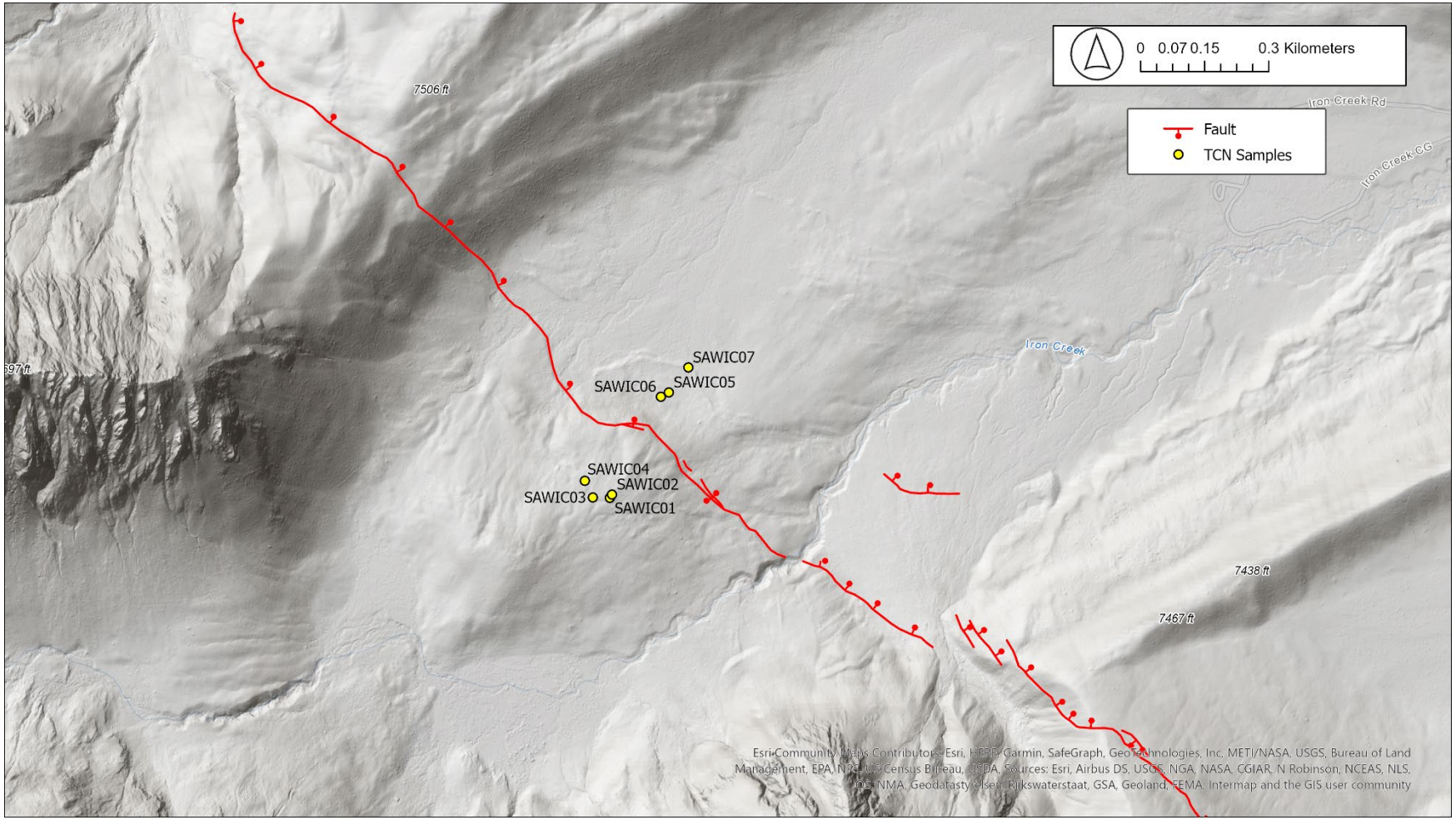

Figure 2. Lidar hillshade map of the Iron Creek Site showing mapping of the Sawtooth fault and locations of TCN samples.

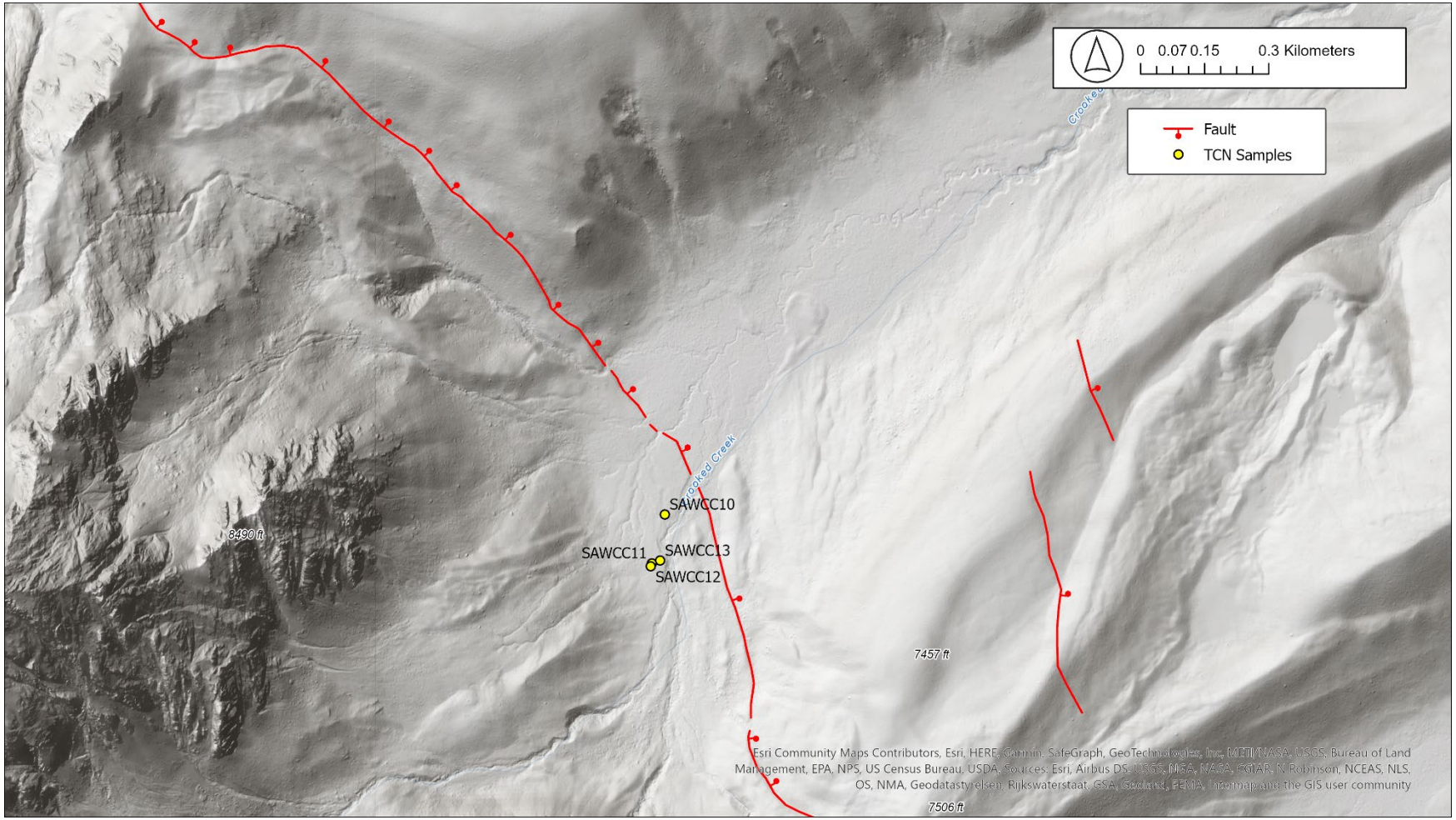

Figure 3. Lidar hillshade map of the Crooked Creek Site showing mapping of the Sawtooth fault and locations of TCN samples.

Figure 4. Lidar hillshade map of the Smiley Creek Site showing mapping of the Sawtooth fault and locations of TCN samples.

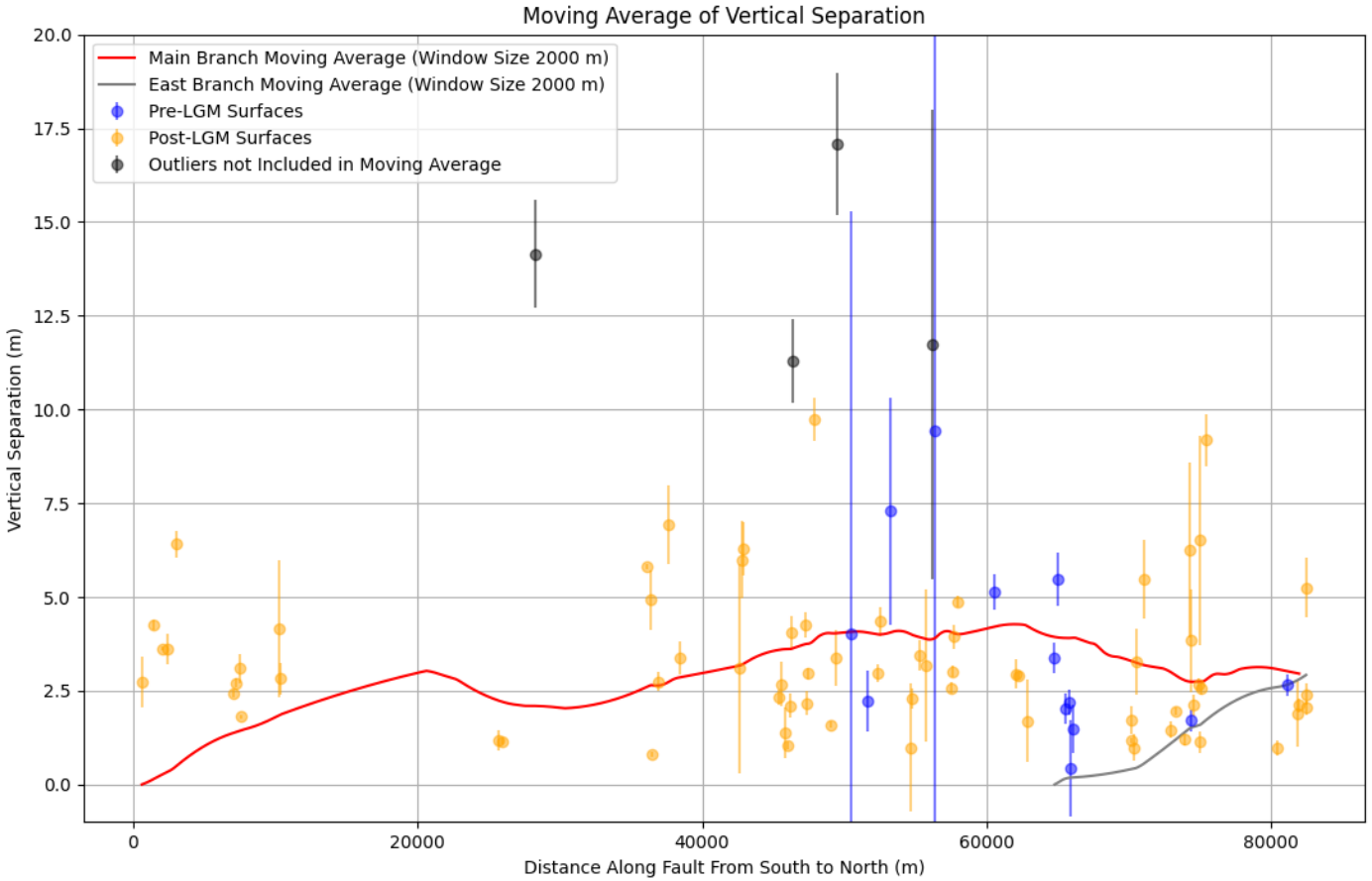

Figure 5. Distribution of vertical separation measurements along the Sawtooth fault. Points and error bars represent the median vertical separation and 1σ uncertainty measured from topographic profiles. Points are colored by age category. The red line is the moving average of measurements along the main branch; the gray line is the moving average of measurements along the east branch. Note that moving average window underestimates values on the left side of the graph.

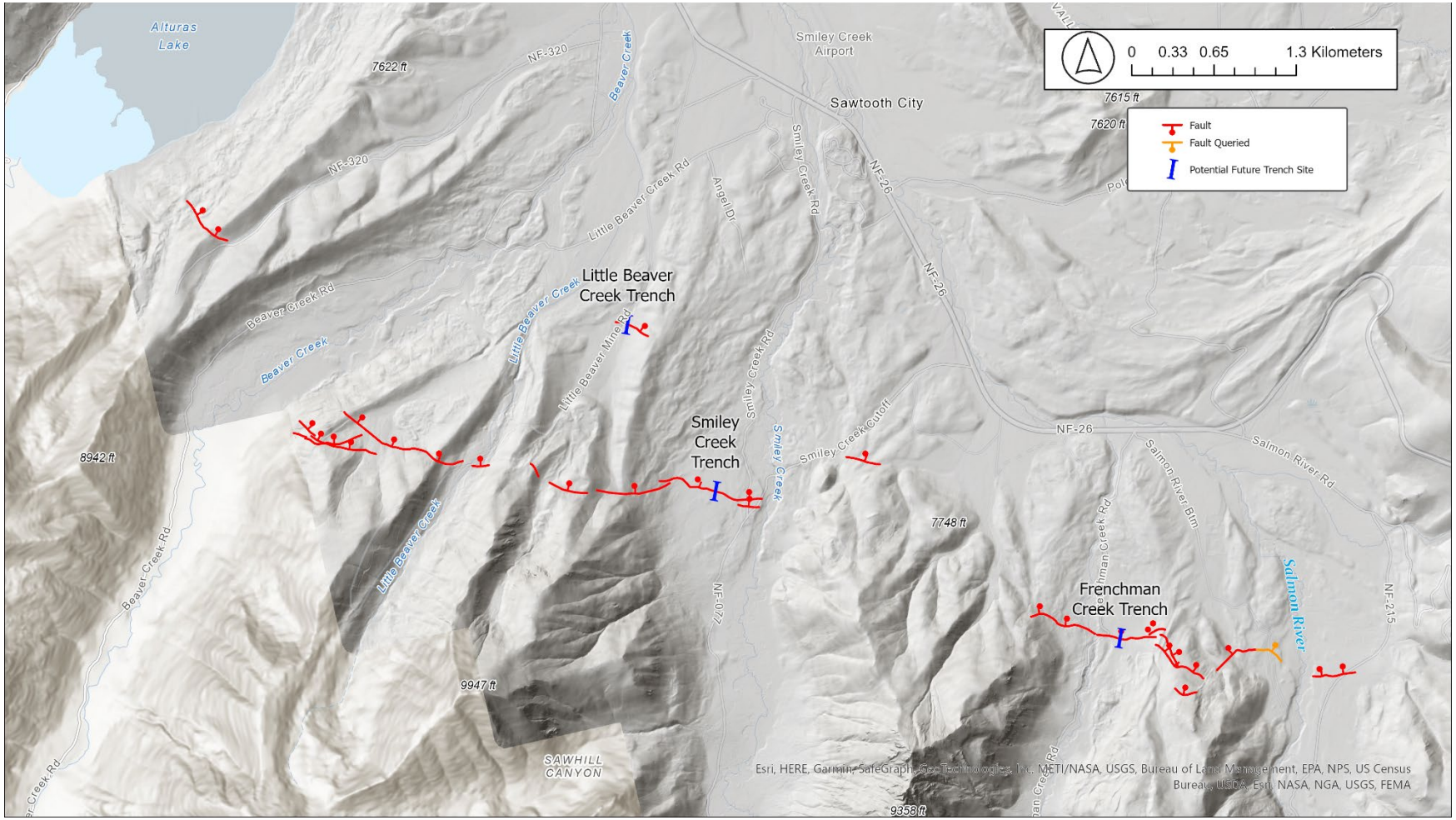

Figure 6. Lidar hillshade and fault mapping along the Salmon River-Alturas Lake section of the Sawtooth fault. Blue lines indicate potential future paleoseismic trench sites.

Figure 7. Field photograph of fault scarp at Smiley Creek. Truck is parked on upper surface and geologist is standing on lower surface.

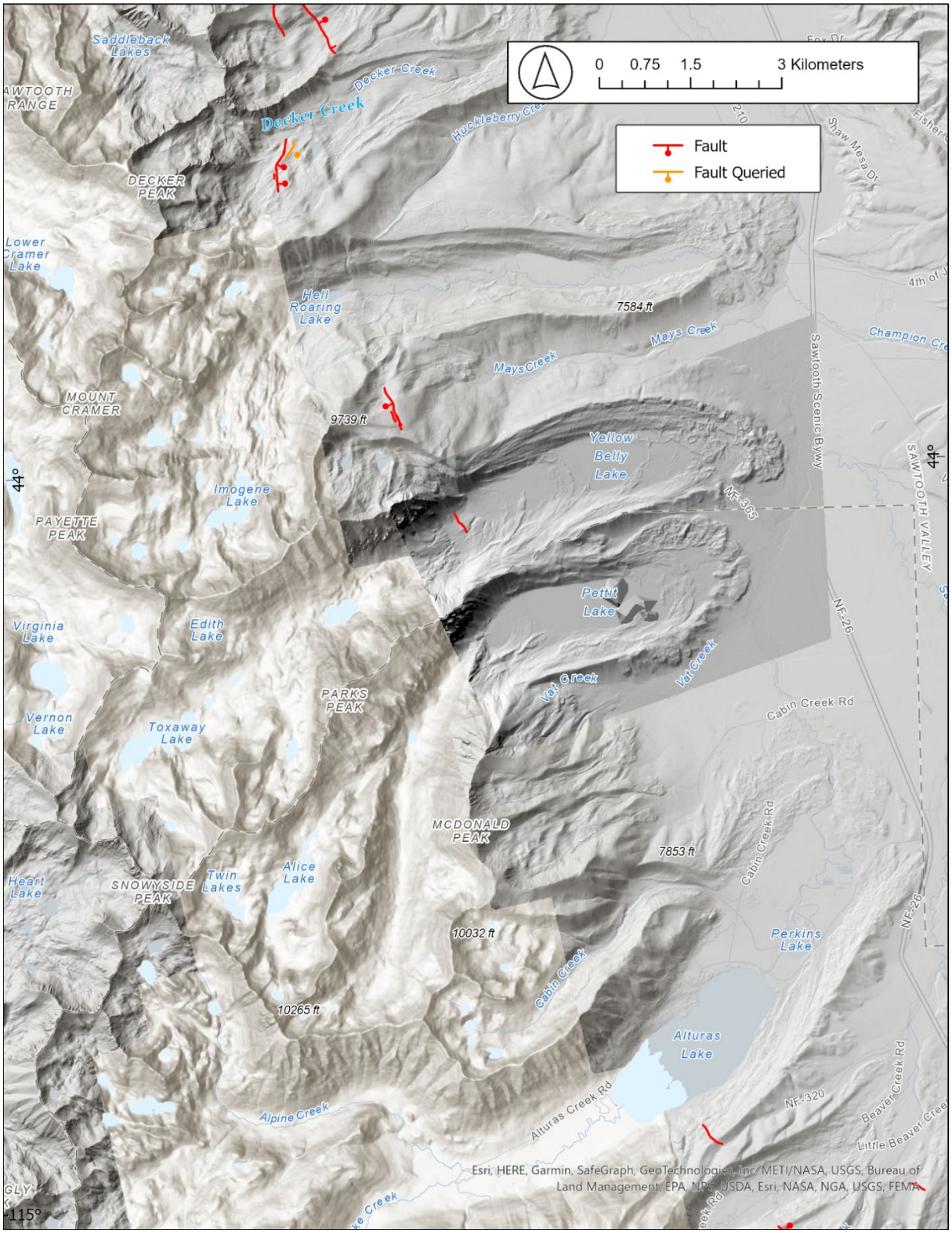

Figure 8. Lidar hillshade and fault mapping along the Alturas Lake-Decker Lake section of the Sawtooth fault.

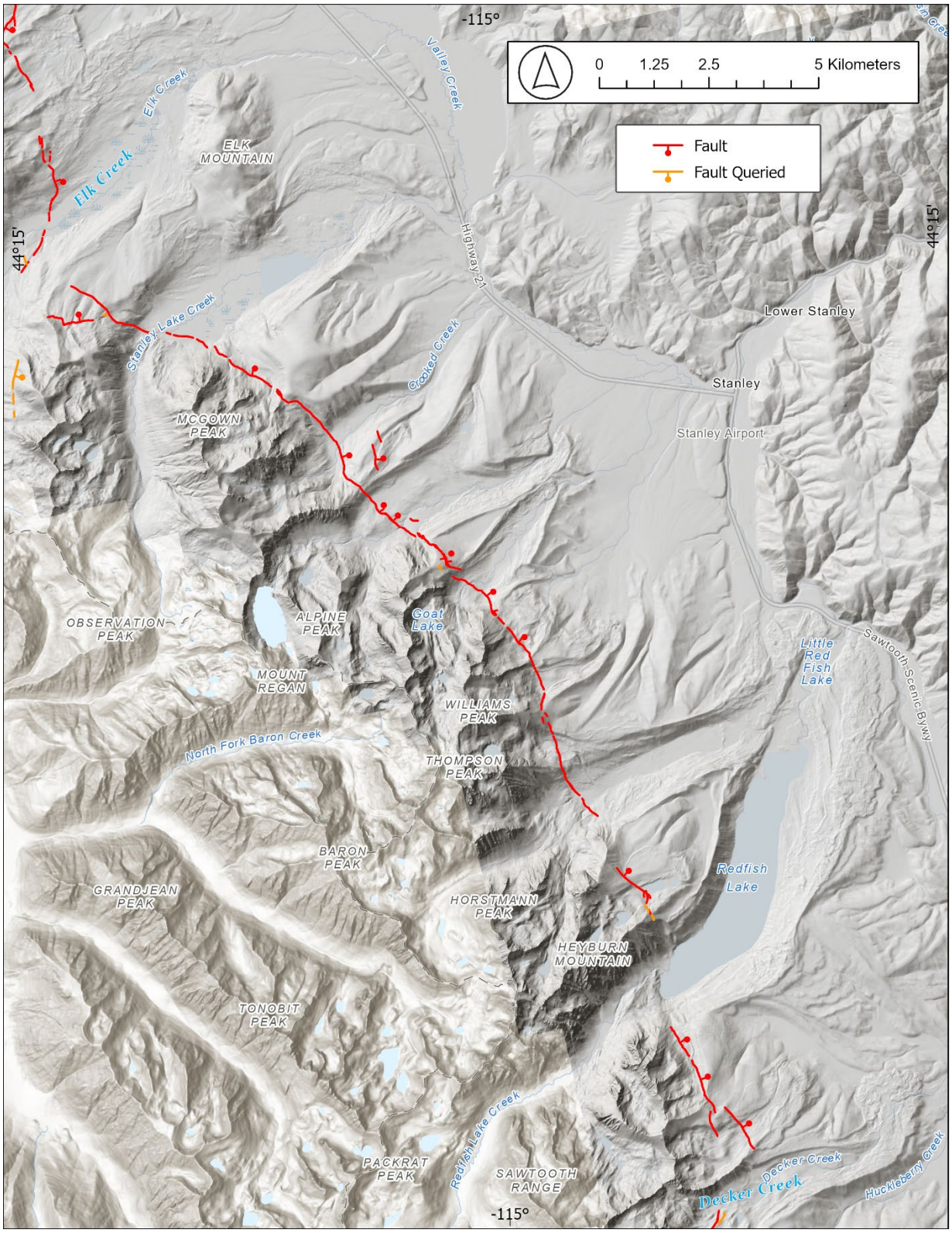

Figure 9. Lidar hillshade and fault mapping along the Decker Lake-Stanley Lake section of the Sawtooth fault.

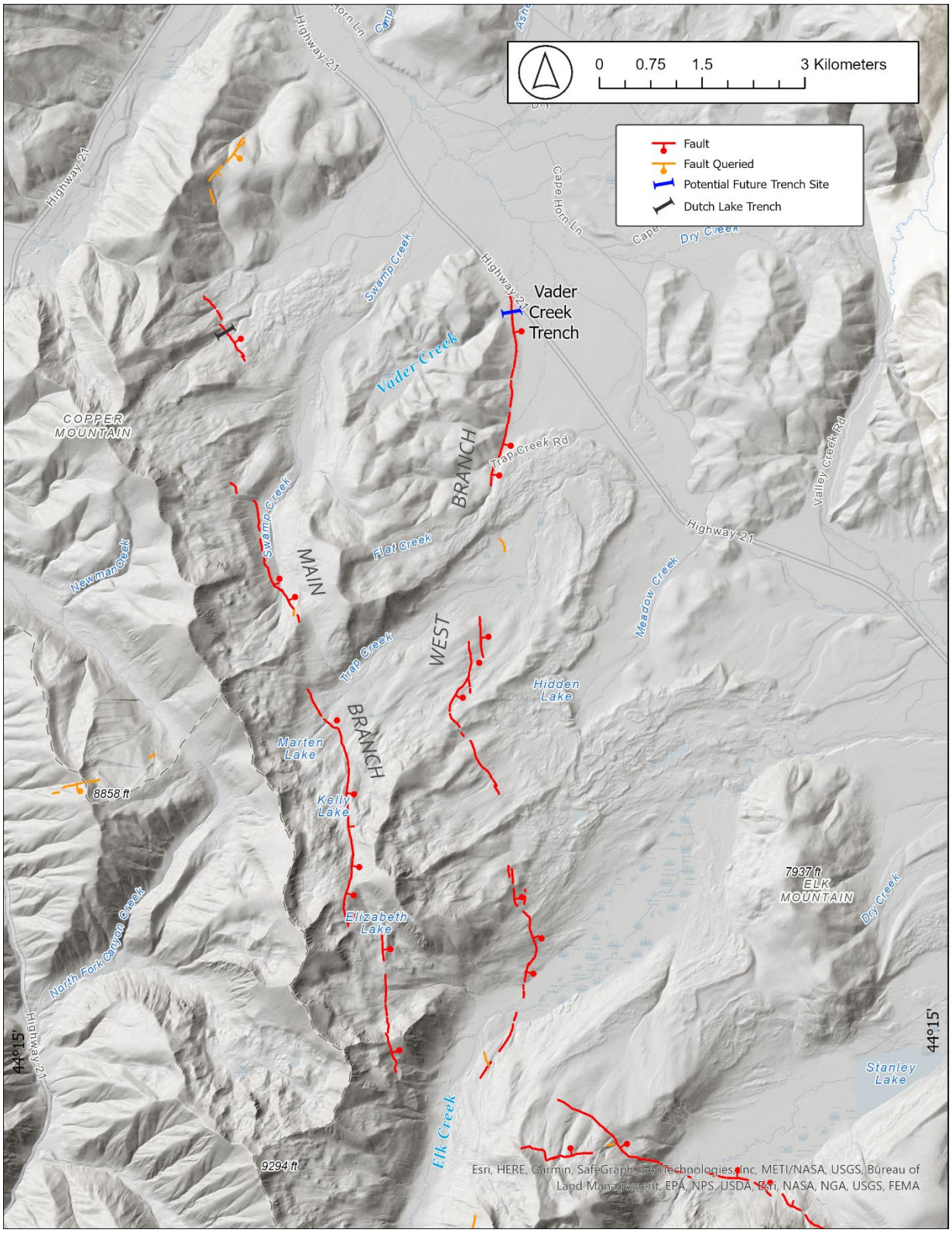

Figure 10. Lidar hillshade and fault mapping along the Stanley Lake-Thatcher Creek section of the Sawtooth fault. Blue lines indicate potential future paleoseismic trench sites.

Figure 11. Field photograph of the Sawtooth fault scarp displacing the Vader Creek alluvial fan. Geologist is standing on the lower alluvial fan surface.

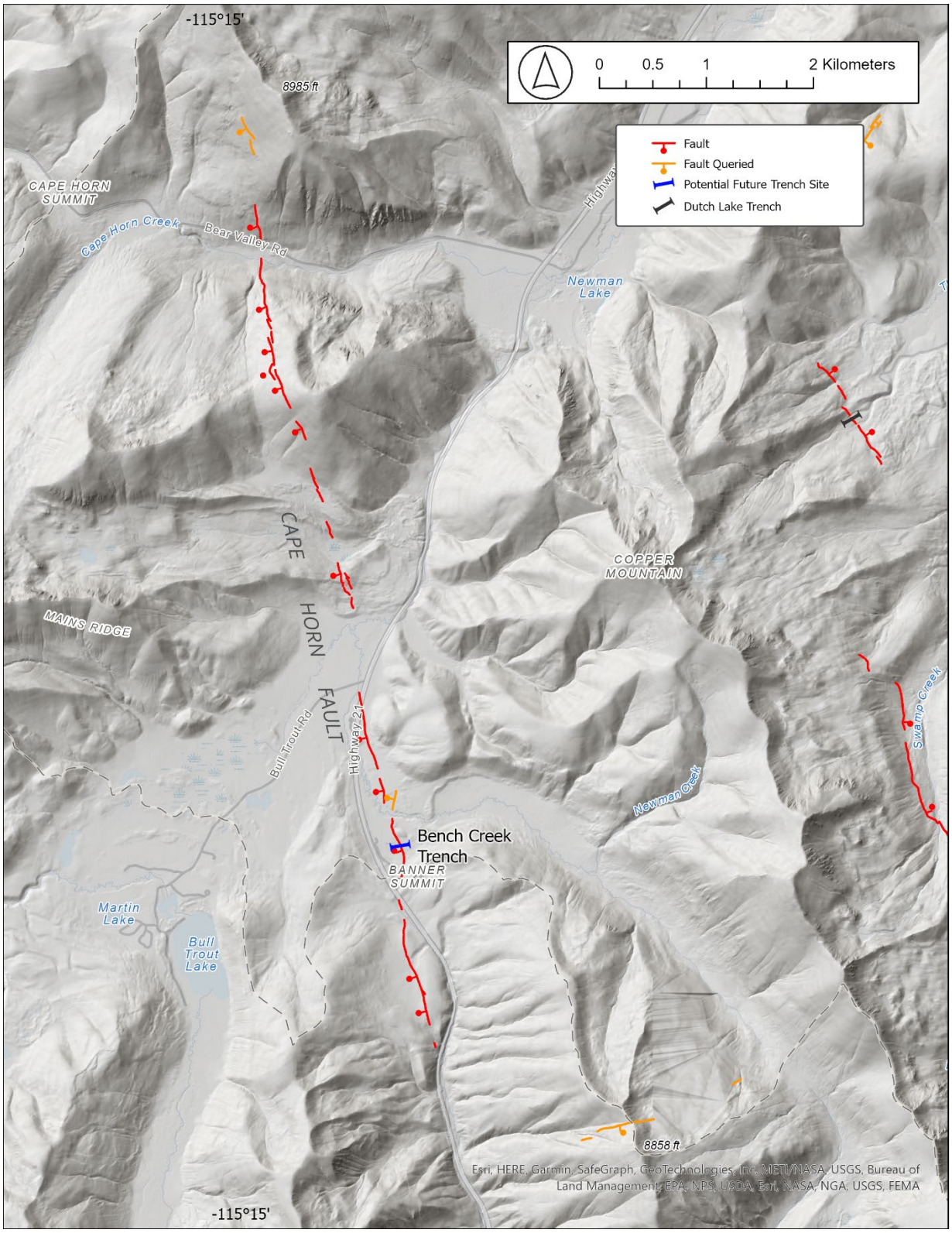

Figure 12. Lidar hillshade and fault mapping along the Cape Horn fault. Blue lines indicate potential future paleoseismic trench sites.

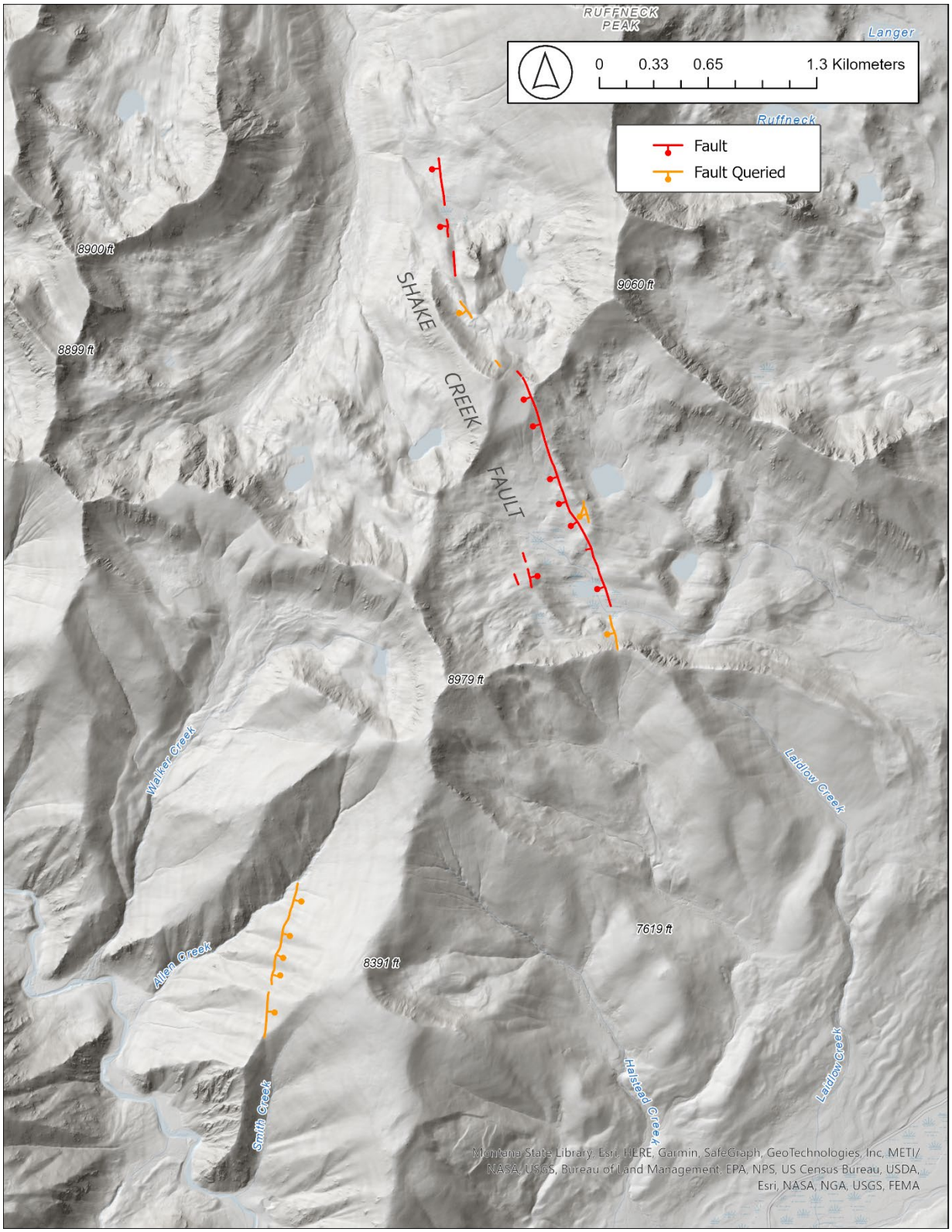

Figure 13. Lidar hillshade and fault mapping along the Shake Creek fault.

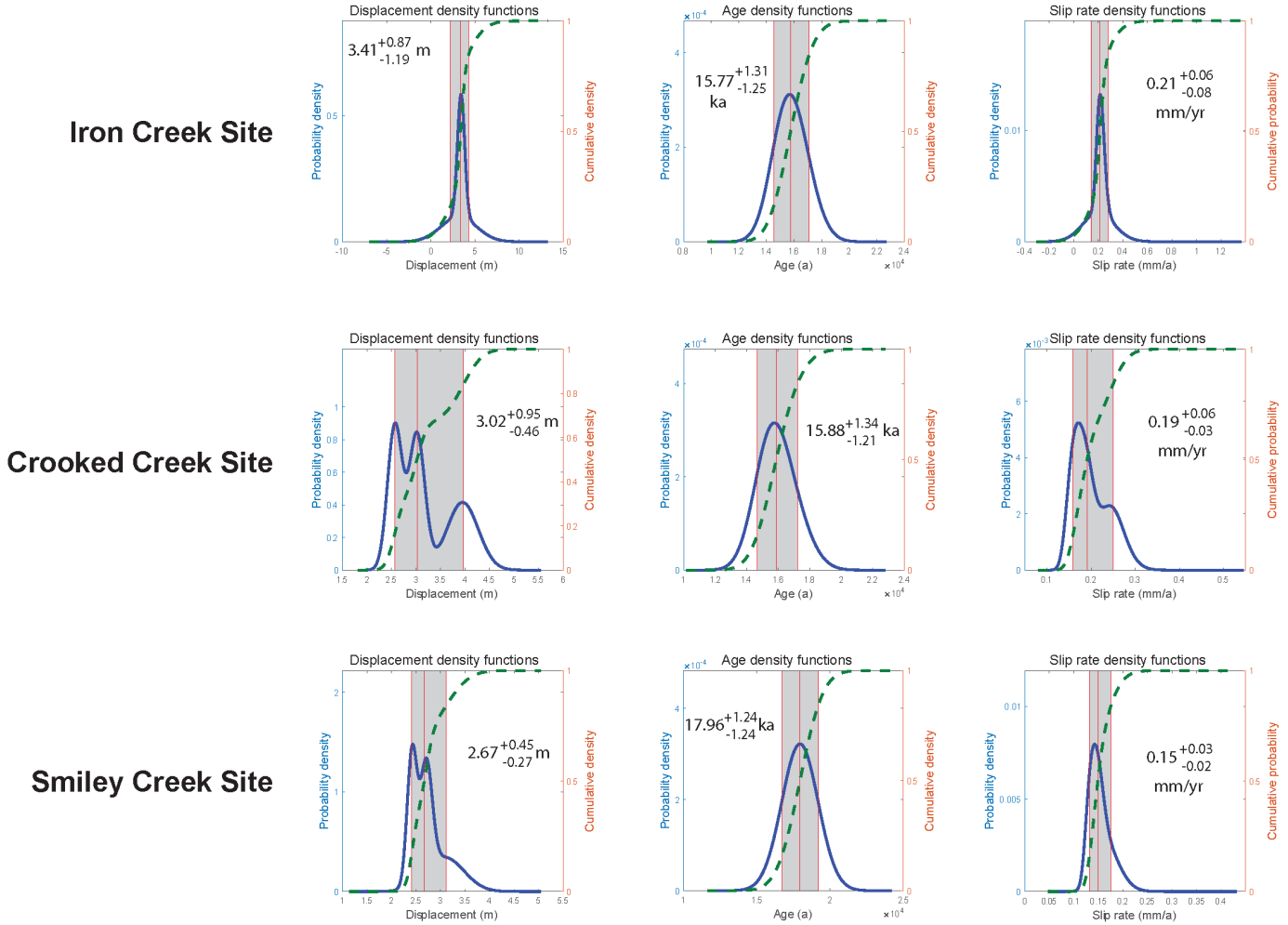

Figure 14. Probability density functions of displacement (left column), age (center column), and slip rate (right column) calculated following Zechar and Frankel (2009). Blue lines are probability density function, dashed green lines are cumulative density function. Vertical red lines are the median and 1σ uncertainty bounds (also shaded gray). We report results with two decimal places here because some values are very low. However, this is not the true precision as these are not significant figures. One decimal place (i.e. tenths of mm/yr) is a more realistic and appropriate level of precision for these results and we round results to that level when discussing them in the text. For slip rate uncertainty results less than 0.1 mm/yr that do not round up, we default to a value of 0.1 since uncertainty cannot be zero and 0.1 mm/yr is the lowest meaningful value.

APPENDIX A

CRONUS Online Exposure Age Calculator Results

Online exposure age calculator v3 results

Version info:

wrapper: 3.0.2
get_age: 3.0.2
muons: 1A, alpha = 1
validate: validate_v3_input.m - 3.0
consts: 2020-08-26

Diagnostics:

Calibration data:

Calibration data set: Default calibration data set

Trace string:

Exposure age results:

Sample name	Nuclide	St			Lm			LSDn			Ag	
		Age (yr)	Interr (yr)	Exterr (yr)	Age (yr)	Interr (yr)	Exterr (yr)	Age (yr)	Interr (yr)	Exterr (yr)	Age (yr)	Interr (yr)
SAWIC01	Be-10 (qtz)	16764	355	1511	16336	345	1398	16063	339	1100	--	--
SAWIC02	Be-10 (qtz)	15345	328	1372	15016	320	1276	14770	315	1005	--	--
SAWIC03	Be-10 (qtz)	16057	339	1440	15671	330	1335	15401	323	1050	--	--
SAWIC04	Be-10 (qtz)	15899	367	1433	15522	358	1330	15228	350	1047	--	--
SAWIC05	Be-10 (qtz)	16398	299	1464	15993	291	1355	15752	286	1063	--	--
SAWIC06	Be-10 (qtz)	17644	376	1599	17156	364	1476	16903	358	1163	--	--
SAWIC07	Be-10 (qtz)	17108	313	1534	16655	303	1417	16420	299	1113	--	--

Summary statistics:

St scaling, all nuclides

All data: mean 16459; SD 779; chi-squared p-value is 0.0000.
Pruned 2 outliers.
Remaining data have p greater than 0.05; using error-weighted mean.
Summary value is 16475 +/- 148 (1448).
If this is a moraine, the probability that it is Younger Dryas age is 0.01.
The probability it belongs to the Antarctic Cold Reversal is 0.10.

Lm scaling, all nuclides

All data: mean 16050; SD 726; chi-squared p-value is 0.0001.
Pruned 2 outliers.
Remaining data have p greater than 0.05; using error-weighted mean.
Summary value is 16064 +/- 144 (1337).
If this is a moraine, the probability that it is Younger Dryas age is 0.01.
The probability it belongs to the Antarctic Cold Reversal is 0.14.

LSDn scaling, all nuclides

All data: mean 15791; SD 732; chi-squared p-value is 0.0001.
Pruned 2 outliers.
Remaining data have p greater than 0.05; using error-weighted mean.
Summary value is 15804 +/- 142 (1037).
If this is a moraine, the probability that it is Younger Dryas age is 0.00.
The probability it belongs to the Antarctic Cold Reversal is 0.14.

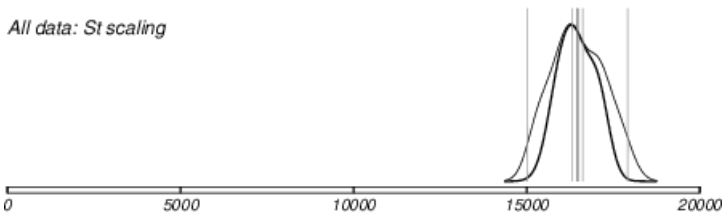

Postscript file -- GMT script

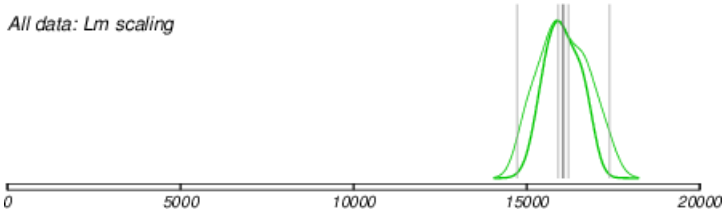

Postscript file -- GMT script

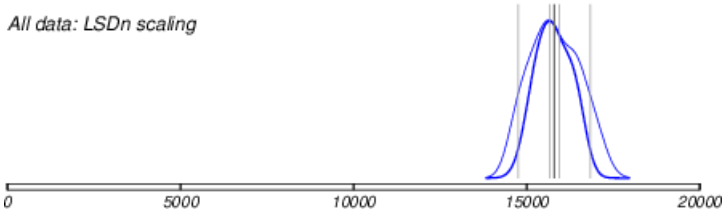

Postscript file -- GMT script

Online exposure age calculator v3 results

Version info:

wrapper: 3.0.2
get_age: 3.0.2
muons: 1A, alpha = 1
validate: validate_v3_input.m - 3.0
consts: 2020-08-26

Diagnostics:

Calibration data:

Calibration data set: Default calibration data set

Trace string:

Exposure age results:

Sample name	Nuclide	St			Lm			LSDn			Ag	
		Age (yr)	Interr (yr)	Exterr (yr)	Age (yr)	Interr (yr)	Exterr (yr)	Age (yr)	Interr (yr)	Exterr (yr)	Age (yr)	Interr (yr)
SAWSC08	Be-10 (qtz)	19052	350	1728	18444	337	1586	18042	329	1234	--	--
SAWSC09	Be-10 (qtz)	18853	412	1723	18260	398	1583	17864	388	1239	--	--

Summary statistics:

St scaling, all nuclides

All data: mean 18953; SD 141; chi-squared p-value is 0.7118.
Pruned 0 outliers.
Remaining data have p greater than 0.05; using error-weighted mean.
Summary value is 18969 +/- 267 (1705).

Lm scaling, all nuclides

All data: mean 18352; SD 130; chi-squared p-value is 0.7245.
Pruned 0 outliers.
Remaining data have p greater than 0.05; using error-weighted mean.
Summary value is 18367 +/- 257 (1564).

LSDn scaling, all nuclides

All data: mean 17953; SD 126; chi-squared p-value is 0.7268.
Pruned 0 outliers.
Remaining data have p greater than 0.05; using error-weighted mean.
Summary value is 17967 +/- 251 (1210).

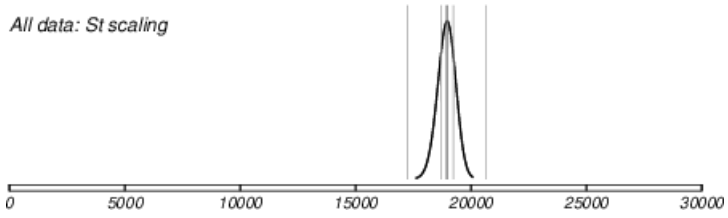

Postscript file -- GMT script

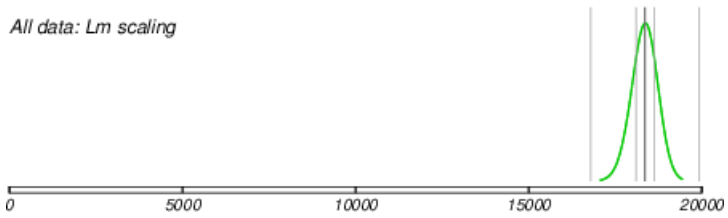

Postscript file -- GMT script

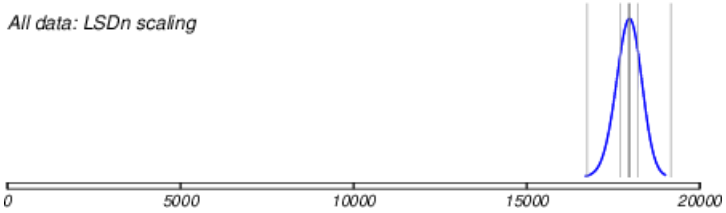

Postscript file -- GMT script

Online exposure age calculator v3 results

Version info:

wrapper: 3.0.2
get_age: 3.0.2
muons: 1A, alpha = 1
validate: validate_v3_input.m - 3.0
consts: 2020-08-26

Diagnostics:

Calibration data:

Calibration data set: Default calibration data set

Trace string:

Exposure age results:

Sample name	Nuclide	St			Lm			LSDn			Ag	
		Age (yr)	Interr (yr)	Exterr (yr)	Age (yr)	Interr (yr)	Exterr (yr)	Age (yr)	Interr (yr)	Exterr (yr)	Age (yr)	Interr (yr)
SAWCC10	Be-10 (qtz)	17655	371	1598	17167	359	1475	16966	355	1166	--	--
SAWCC11	Be-10 (qtz)	15953	341	1431	15574	332	1328	15382	328	1050	--	--
SAWCC12	Be-10 (qtz)	15916	302	1419	15540	295	1316	15348	291	1037	--	--
SAWCC13	Be-10 (qtz)	16646	376	1504	16230	365	1394	16015	360	1103	--	--

Summary statistics:

St scaling, all nuclides

All data: mean 16542; SD 814; chi-squared p-value is 0.0011.
Pruned 1 outlier.
Remaining data have p greater than 0.05; using error-weighted mean.
Summary value is 16122 +/- 194 (1420).
If this is a moraine, the probability that it is Younger Dryas age is 0.01.
The probability it belongs to the Antarctic Cold Reversal is 0.14.

Lm scaling, all nuclides

All data: mean 16128; SD 762; chi-squared p-value is 0.0019.
Pruned 1 outlier.
Remaining data have p greater than 0.05; using error-weighted mean.
Summary value is 15735 +/- 189 (1314).
If this is a moraine, the probability that it is Younger Dryas age is 0.01.
The probability it belongs to the Antarctic Cold Reversal is 0.20.

LSDn scaling, all nuclides

All data: mean 15928; SD 757; chi-squared p-value is 0.0017.
Pruned 1 outlier.
Remaining data have p greater than 0.05; using error-weighted mean.
Summary value is 15537 +/- 186 (1026).
If this is a moraine, the probability that it is Younger Dryas age is 0.00.
The probability it belongs to the Antarctic Cold Reversal is 0.20.

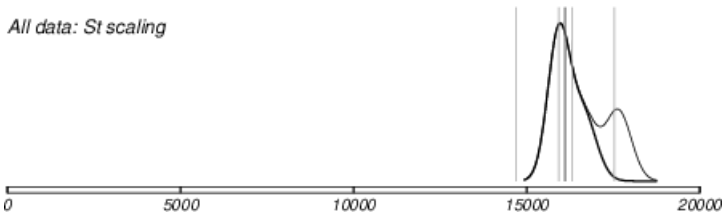

Postscript file -- GMT script

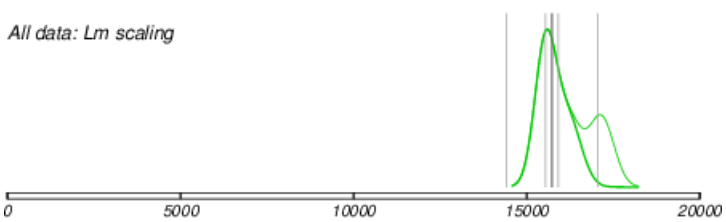

Postscript file -- GMT script

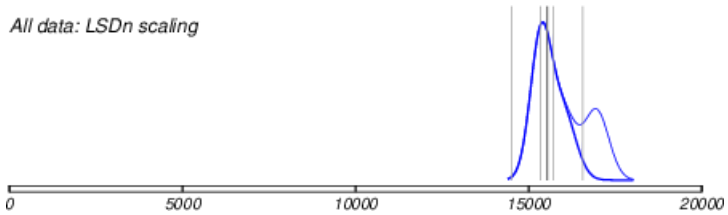

Postscript file -- GMT script